university of groningen

University of Groningen
Faculty of Mathematics and Natural Sciences
Zernike Institute
Quantum interactions and structural dynamics

X-Ray photoionization of DNA-nanoparticle complexes

6/22/2016
University of Groningen
E. Castellano Altable

Table of Contents

Abstract

The radiotherapy treatment based on high-energy photons is nowadays commonly used to treat cancer.

There are numerous theoretical studies that have been carried out investigations on the viability of metal nanoparticles as contrast agents in radiotherapy treatments. These studies have shown that the relative dose to tissue volumes can be significantly increased by the addition of these nanoparticles due to their larger X-ray absorption cross section as compared to biological tissue.

In this project we want to study the processes underlying the interaction between photons and a complex consisting of a metal nanoparticle and DNA. In particular it will be investigated whether Auger electrons are playing a crucial role in this interaction, as many studies suggest.

In order to bring the major conclusions within thin this context, we have carried out experiments related to the fragmentation of DNA strands induced by soft X-ray photoionization and photoexcitation. Furthermore, novel approaches for the production of complexes of small functionalized Ag_N:DNA were investigated.

1. Introduction

The study of radiation action on biological tissue begun with three different experiments done by three scientists. In 1895 Wilhelm Conrad Röntgen discovered a "magic" radiation that could penetrate solid objects. He called this radiation ~~x~~-rays, since they were a real mystery to him. One year later when Henri Becquerel was experimenting with a uranium salt, ~~he~~ he noticed that the photographic material, close to the cupboard he used to use to put the uranium, had been exposed to radiation uranium salt and many spots had appeared on the material. Finally in 1898 the Curies discovered the elements polonium (Po) and radium (Ra) and coined the term radioactivity. The Curies and Becquerel would share the Nobel Prize in 1903 for this discoveries

The medical community quickly recognized the therapeutic power of this "radiation". For instance in 1896 Despegines used X-Ray treatment for the first time to treat patients suffering from stomach cancer.

In the following years the immediate effects of high doses of ioniz~~ation~~ radiation upon the human body were well studied. Scientists divided the effects in two categories; the acute effects produced by high doses which appears soon after the exposure (e.g. the bone marrow or the neurovascular syndromes) and the late effects which, even with low doses, can appear many years after the exposure. An example for a late effect is radiation induced cancer.

It is nowadays well established that the main biological radiation damage can be attributed to DNA damage. Many research groups from the field of medicine, radiobiology ~~and~~ radiation chemistry, and also molecular physics ~~have aspects of~~ radiation induced DNA damage.

The main goal of radiotherapy is to provide tumour control by killing cancerous cells using ionizing radiation while simultaneously sparing surrounding tissues, with the ultimate goal of eradication of all malignous cells.

In current medical practice, a large difference between dose to the tumour and dose to the surrounding tissue is typically achieved through spatially shaping the dose around the tumour, typically through the use of multiple modulated radiation fields (an example is Intensity Modulated Radiation Therapy (IMRT)). However, the dose ratio achievable between a tumour and surrounding healthy tissues is ultimately limited by their very similar X-ray absorption characteristics.

An alternative method which has received increasing interest in recent years is the use of heavy atoms as contrast agents. Heavier elements increase the dose delivered to surrounding tissues due to their greater mass energy absorption coefficients, and can thus potentially improve the contrast between healthy and cancerous cells if they can be preferentially delivered to tumors. They are what we call radiosensitizer. [4]

The heavy atoms can be administered as salts, contained in other molecules or even as nanoparticles. However, the nanoparticles ~~form~~ has shown some advantages, ~~essentially~~ that they can be functionalized. Biocompatible molecules are put on the surface of the NPs, ~~this~~ allows ~~us~~ to control (to some extent) where the particle go and what they interact with.

For this reason, numerous theoretical studies have been carried out investigating the viability of metal nanoparticles as contrast agents, and have shown that the dose to tissue volumes can be significantly increased by the addition of such nanoparticles due to their greater X-ray absorption. [5]

For example for the case of gold nanoparticles (GNPs) concentrations of the order of 1% ~~mass~~ have been ~~suggested~~ to increase the dose deposited by up to a factor of two, which suggests considerable potential for increasing cell killing through the selective delivery of gold nanoparticles. [2] The underlying process is still under investigation. However some studies suggest that the enhanced is produced by the Auger cascade produced by the incoming photons.

The aim of this thesis is to study of the interaction between complexes of metal NPs and strands of DNA with soft X-rays on the molecular level, i.e. for free complexes in the gas phase. For this purpose we have conducted two independent studies: ~~Initially~~ we made efforts to obtain molecular complexes formed by silver nanoparticles and DNA strands (see section 3). ~~In addition, we further~~ studied the ionization-induced fragmentation of a single DNA strand in the gas phase (see section 4).

2. Fundamentals

2.1 High Performance Liquid Chromatography - HPLC

To obtain, identify and collect pure Ag:DNA compounds we have used a technique known as high-performance liquid chromatography [1] . HPLC is an established technique that is used to separate, identify, and quantify components in a mixed solution.

A pressurized liquid solvent containing the sample mixture is at the basis of the HPLC technique. The solution is pushed through a column filled with an adsorbent solid material by means of a powerful pump. Each component of the mixture interacts differently with the adsorbent material causing different flow rates, or retentions times, for each component. As a result, one can separate the different components of the mixture. The active component of the column, the absorbent, is typically a granular material made of solid particles (e.g. silica, polymers, etc.), 2–50 micrometers in size.

The sample is typically composed of the mixture we want to separate and solvents (Water, Methanol) which are called the mobile phases. The composition and the temperature play a role in the separation processes because they influence the interaction between the components and the absorbent material. The interactions process may be either hydrophobic, dipole, dipole-dipole, ionic, and most often a combination of tow or more.

In the following figure, a schematic drawing of an HPLC system is shown. It consist of: pumps, sampler, and detector. The sampler takes the sample mixture into the mobile phase stream and carries it into the column. The pumps then pushes the desired flow composition of the mobile phase through the column. Then, the detector generates a signal which is proportional to the amount of sample component coming out from the column. This allows an analysis of the components.

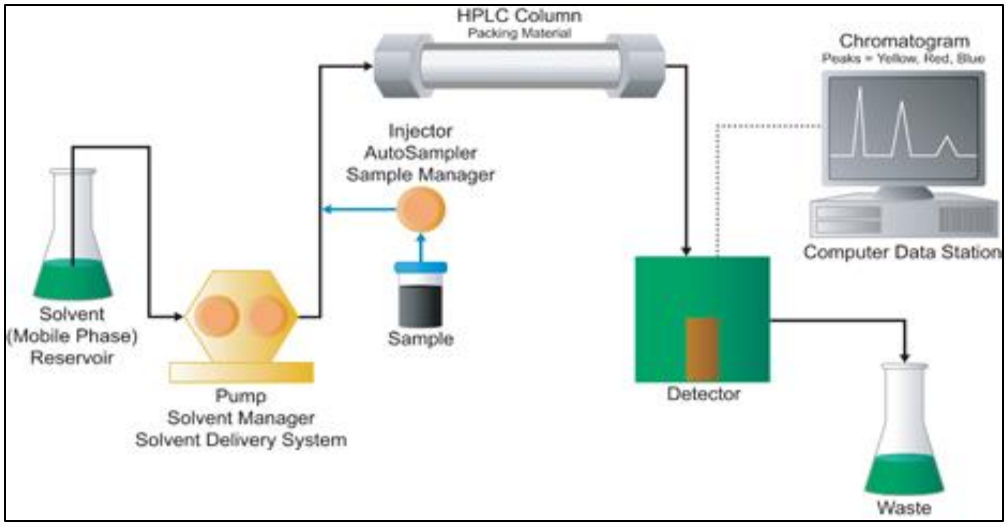

Figure 1: *Schematic draw of the HPLC technique* [1]

The HPLC is controlled by a digital microprocessor and the data analysis is ~~made at the~~ user software controller. Various detectors are in common use, such as (ultraviolet detectors), photodiode arrays (PDA) or based on mass spectrometry. Most HPLC instruments have a column oven which is used to adjust the temperature of the separation performance.

In practice ~~process~~ is the following: the sample mixture to be separated and analyzed is introduced into the stream of mobile phase through the column. The components of the sample move through the column at different velocities, which depend on the specific physical interactions with the absorbent material.

The velocity of the components through the column depends on its chemical nature, on the nature of the stationary phase (the column), on the composition of the mobile phase, temperature and pressure will play an important role. The time at which a specific analyte emerges from the column is called its retention time. The identifying characteristic of a given analyte is the retention time (measured under specific conditions) and allows the separation of different components.

There are two operation modes depending whether the composition of the mobile phase is kept constant 1) isocratic elution mode and 2) ~~varied~~ ~~(~~"gradient elution mode"~~)~~ during the chromatographic analysis.

In the second mode the composition of the mobile phase varies typically from low to high eluting strength. The eluting strength of the mobile phase is reflected by analyte retention times with high eluting strength producing fast elution (=short retention times).

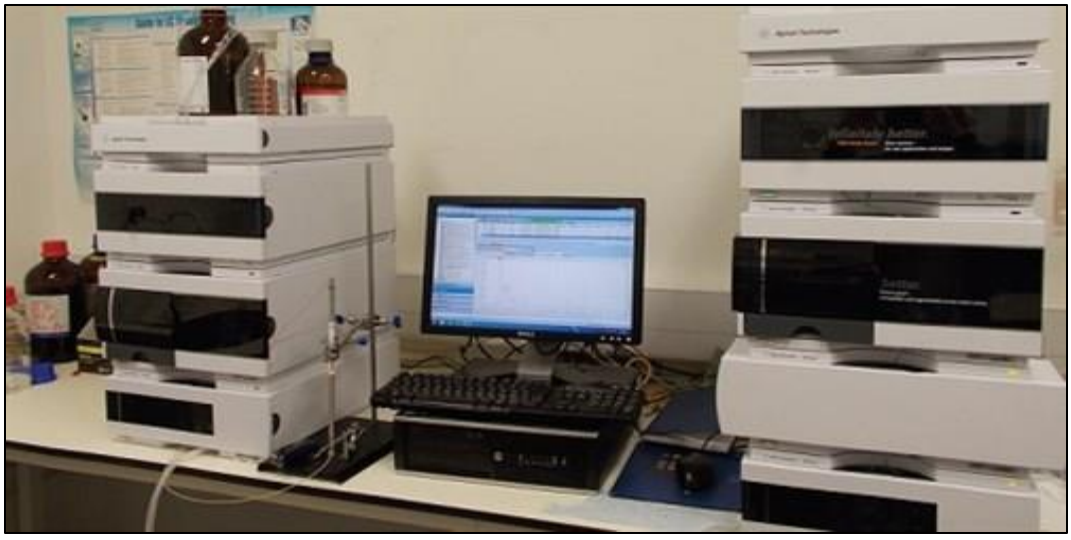

***Picture 1**: ~~Real~~ HPCL System, similar to the one used [1]*

2.2 Electrospray Ionization Source (ESI) - PAULTJE

During this work we wanted to study soft X-Ray induced radiation damage to gas phase oligonucleotide ions. To this end, oligonucleotides have to be transferred into the gas phase using the tandem mass spectrometer Paultje. [6]

Paultje is a home-built setup which allows us to study the dynamics of biomolecular ions. Briefly, oligonucleotide are produced by an electrospray ionization source (ESI) from a solution and stored in an ion trap at low pressures (10^{-6} – 10^{-7} mbars). The electrosprayed molecules enter in the first vacuum section of the setup through a small capillary tube and are then transported through a RF ion funnel, an RF octopole ion guide and a quadrupole mass filter to the three dimensional ion trap. The trapped molecules are then exposed to soft X-Ray photons and the collision products are extracted into a TOF spectrometer and detected by a microchannel plate detector (MCP).

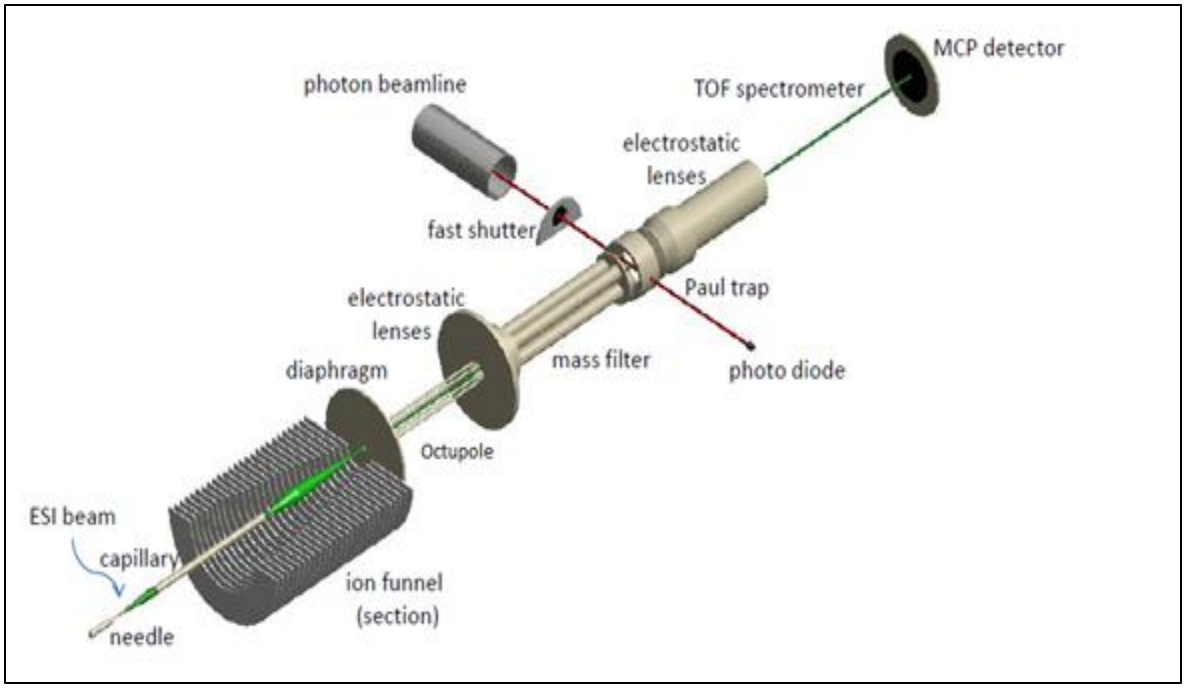

Figure 2: *Schematic drawing of Electrospray ionization Source (ESI) setup - Paultje: Green line represents the ions path, red lines represents the soft X-ray Beam.*[9]

Now we proceed to describe the detailed description of the different stages of the setup:

2.2.1 ESI

Electrospray Ionization (ESI) is a method by which solute molecules present in a solution can be transferred into the gas phase as ions. The gas-phase ions can then be manipulated and detected by mass spectrometric means. The significance of ESI-MS was recognized by the award of a Nobel Prize in 2002 to John Fenn, who was the major developer of this technique [8]. The initial development of the method is due to Malcolm Dole. [17]

Depending on the pH value, biomolecules in solution may be positive (protonated) or negative (de-protonated) ions, or non-ionic compounds. In the last case, the molecule can be investigated associated with one or more of the ions present in the solution. ~~This charging process is part of the electrospray mechanism.~~

There are three major steps in the production of gas-phase ions from electrolyte ions in solution: (1) production of charged droplets at the ESI capillary tip; (2) shrinkage of the charged droplets due to solvent evaporation and repeated charge-induced droplet disintegrations that ultimately lead to small highly charged droplets capable of producing gas-phase ions, and (3) the actual mechanism by which gas-phase ions are produced from these droplets. We describe these three steps below.

As shown in *figure 3* the chemically ionized molecule in the solution are pumped through the tip of a needle. The capillarity is installed in front of the needle at a distance of 5 mm. A high voltage (typically in the range of 3-5 KeV) is applied to the needle and produces a strong electric field between needle and its capillarity counter electrode. Due to the applied electric field, the solution forms a liquid meniscus at atmospheric pressure and separates between the positive and negative ions. ~~A capillarity is installed in front of the needle at a distance of 5 mm~~

The applied electric field penetrates into the liquid and induces the formation of an electric double layer at the meniscus. The double layer is produced due to the polarizability and dipole moments of the solvent molecules which causes an enrichment of positive ions near the meniscus. This cause a instability of the meniscus ~~and produces~~ of a cone (Taylor cone) and subsequently a jet of droplets charged by the excess of positive ions. The transition from the Taylor cone to the jet of droplets occurs because the charged surface at the tip of the Taylor cone avoids turning into an infinitesimally sharp tip that would constitute and electric field singularity.

When the electric field applied is negative, the jet splits into droplets charged with an excess of positive ions. Evaporation of the charged droplets brings the charges closer together. When the increasing coulombic repulsion is higher than the surface tension (Rayleigh limit) the droplets emit a jet of smaller charged progeny droplets. Evaporation of progeny droplets leads to de stabilization and emission of a second generation of progeny droplets, and so on until free gas-phase ions form at some point.

The last mechanism of the formation of the gas-phase ions can be described by two models. The Ion Evaporation model (IEM) and the Charge Residue Model (CRM).

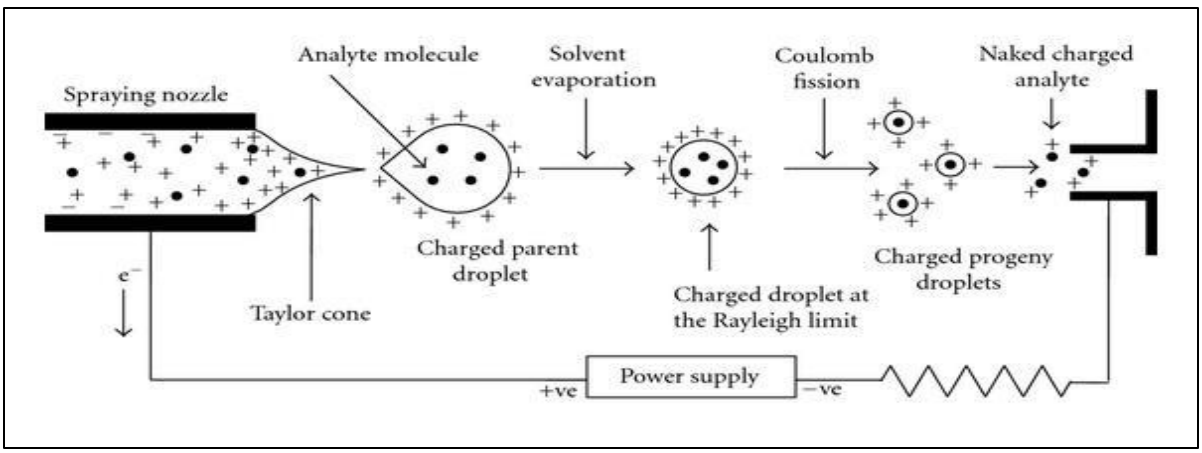

Figure 3: *Schematic of the electrospray process* [19]

The IEM suggests that as the droplet reaches a certain radius the field strength at the surface of the droplet becomes large enough to assist the field desorption of solvated ions.

The CRM states that electrospray droplets undergo evaporation and fission cycles, eventually leading to progeny droplets that contain on average one analyte ion or less. The gas-phase ions form after the remaining solvent molecules evaporate, leaving the analyte with the charges that the droplet carried.

All these stages occur in the atmospheric pressure region of the apparatus (see *Figure 3)*. A small fraction of the ions resulting from the preceding stages enter the vacuum region of the interface leading to the mass spectrometer through the capillary.

The gas-phase ions can be clustered with solvent molecules and other additives which must be removed. The gas-phase ions are therefore subjected to a thermal declustering or clean-up stage by heating the capillary which also avoid sticking ~~to the~~ surfaces.

The chamber past the capillary houses the Ion Funnel, which guides and focuses the ions towards the Paultrap at a pressure lowered by almost 3 orders of magnitude.

2.2.2 Radio Frequency (RF) ION FUNNEL

In many commercial ESI-MS systems, a large fraction of the available ions in the sample are lost before the ions reach the detector. Much of these losses occur in the interface region between the ion source and the entrance to the high vacuum region of the instrument. The use of an RF ion funnel has been shown to reduce these ion losses and improve ~~resultant~~ sensitivity of a mass spectrometer instrument by an average of 6 to 10-fold.

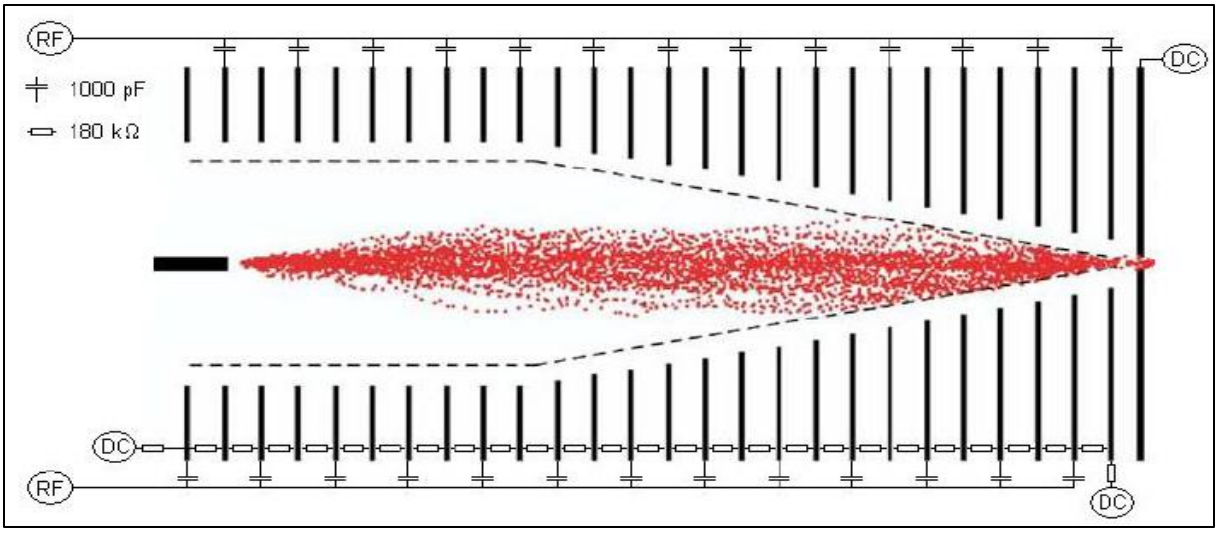

Figure 4*: Schematic draw of the Radiofrequency Ion Funnel*

The ion funnel utilizes a stacked radio frequency (RF) ring electrode arrangement with a funnel shape to focus ions in the presence of a neutral gas [10]. A radiofrequency voltage is applied to the funnel electrodes in a way that neighboring electors are phase shifted by π. This way the RF fields create an effective potential which confines ions in the radial direction.

Inherent to the ion transport is the necessity of slowing the ions down while at the same time focusing the ions sufficiently for maximum transport between the sections. The theorem of Liouville asserts that the phase-space distribution function is constant along the trajectories of the system.

This would imply that decreasing the ion momenta will decrease the beam emittance. This problem is overcome by operation of RF funnel and RF quadrupole at pressures in the range between 1 mbar and 10^{-2} mbar and exploiting the collisional damping of the ion trajectories, which confines ions to the center of the guides. The effect is insignificant in ultrahigh vacuum and disperses the beam at too high a pressure. It is thus beneficial to maintain a relatively high pressure in the ion funnel and first quadrupole chamber, for achieving a high transmission of ions towards the mass filter. [9]

2.2.3 The RF OCTUPOLE ION GUIDE

The electric octupole operating in the r.f.-only mode has been shown to be a powerful tool for guiding ion beams in the energy range from subthermal energies up to few hundred eV. This technique was originally developed by Teloy and Gerlich in 1974 and subsequently octupoles found applications in various fields. [22]

In our home made setup, the function of the Octupole Guide is to lead the ions from the Ion Funnel to the Quadrupole Mass Filter, and help to reduce losses in the transition of the ions from high pressure regions to the low pressure devices such the Paultrap (10^{-6} – 10^{-7} mbars).

2.2.4 QUADRUPOLE MASS FILTER

The Quadrupole mas filter is located between the Between Octupole and the Paultrap. It filter the ions we want to store in the trap.

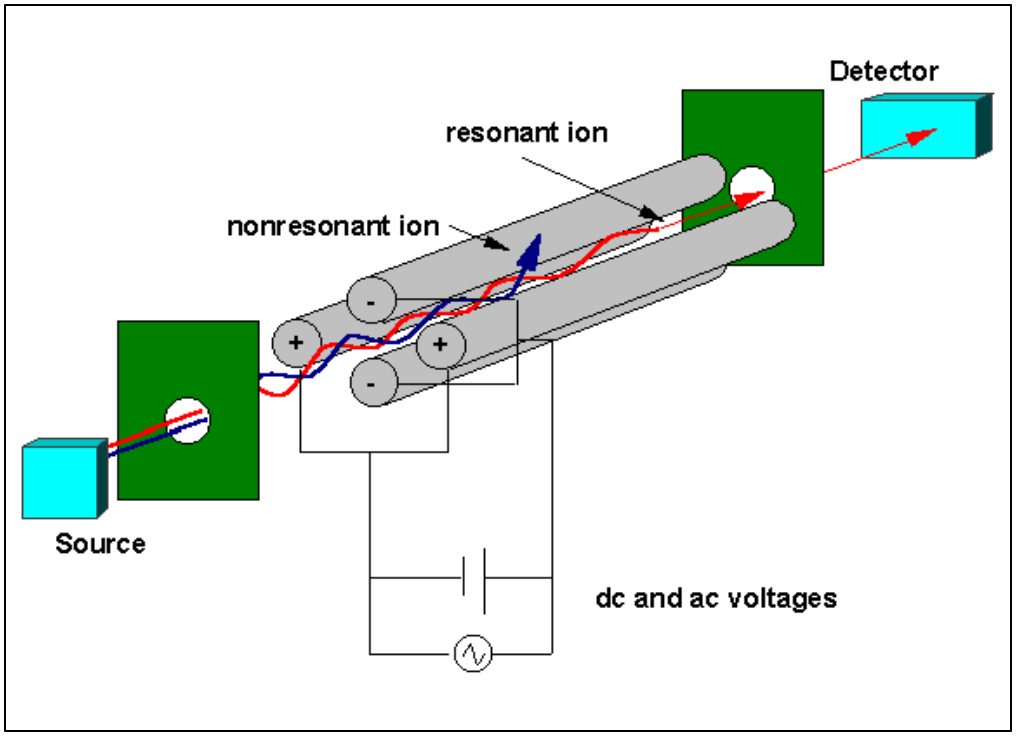

Figure 5: *Schematic draw of a Quadrupole Guide* [20]

A quadrupole mass filter consists of four parallel metal rods arranged as in the *figure 5*. Two opposite rods have an applied potential of $(-U - Vcos(\omega t))$ and the other two rods have a potential of $(U + Vcos(\omega t))$,[11]. The applied voltages affect the trajectory of ions traveling down the flight path centered between the four rods.

For given dc and ac amplitudes, only ions of a certain mass-to-charge ratio pass through the quadrupole filter (resonant ions) while all other ions follow unstable trajectories (non-resonant ions). A mass spectrum is obtained by monitoring the ions passing through the quadrupole mass filter as the voltages on the rods are varied. There are two methods: varying ω and holding U and V constant, or varying U and V with (U/V) fixed for a constant angular frequency, ω.

The general principle of operation of the mass filter can be visualized qualitatively as follows: light ions (low mass to charge ratio) are able to follow the alternating component of the field. For the X-direction, those ions will stay in phase with the RF drive, gain energy from the field and oscillate with increasingly large amplitude until they encounter one of the rods and are discharged. [21]

Therefore the X-direction is a high-pass mass filter: only high masses will be transmitted to the other end of the quadrupole without striking the X-electrodes.

On the other hand, in the Y-direction, heavy ions will be unstable because of the defocusing effect of the DC component, but some lighter ions will be stabilized by the AC component if its magnitude is such as to correct the trajectory whenever its amplitude tends to increase. Thus the Y-direction is a low-pass mass filter: only low masses will be transmitted to the other end of the quadrupole without striking the Y electrodes. By a suitable choice of RF/DC ratio, the two directions together give a mass filter which is capable of resolving individual atomic masses.

The attractive features of the quadrupole as a mass analyzer are evident from the above discussion: the quadrupole mass filter provides a convenient filter which can be tuned to a desired mass by varying the amplitude of the RF voltage, V; the mass window can also be varied electronically by simply adjusting the DC/RF ratio. Simultaneously varying the amplitude of the DC and RF voltages (at fixed ω) allows the entire mass spectrum to be scanned.

2.2.5 RF Ion Trap-~~PAULTRAP~~

After the Quadrupole mass filter a commercial RF ion trap set which includes entrance and exit ion lenses is used to trap the mass-selected ions (Jordan TOF Products, USA). The ion trap consists of a central hyperbolic ring electrode enclosed by two hyperbolic end cap electrodes [7].

The DC voltage is set to 1MHz while the RF amplitude varies depending on the interest range of masses under study. For higher amplitudes, the system is more efficient in trapping large masses but we have a high low-mass cutoff. Meanwhile for low amplitudes the mass cutoff is lower, but the system is less efficiently trapping large masses.

For optimum ion transport from the ion guide into the trap, the ion guide is biased typically to 4 V., Consequently 5–6 eV of kinetic energy, induced in the ions by the RF-Trap, has to be dissipated. To this end we use a Helium buffer gas pulses up to a pressure of ≈ 10–3 mbar, introduced by a solenoid pulsed valve.

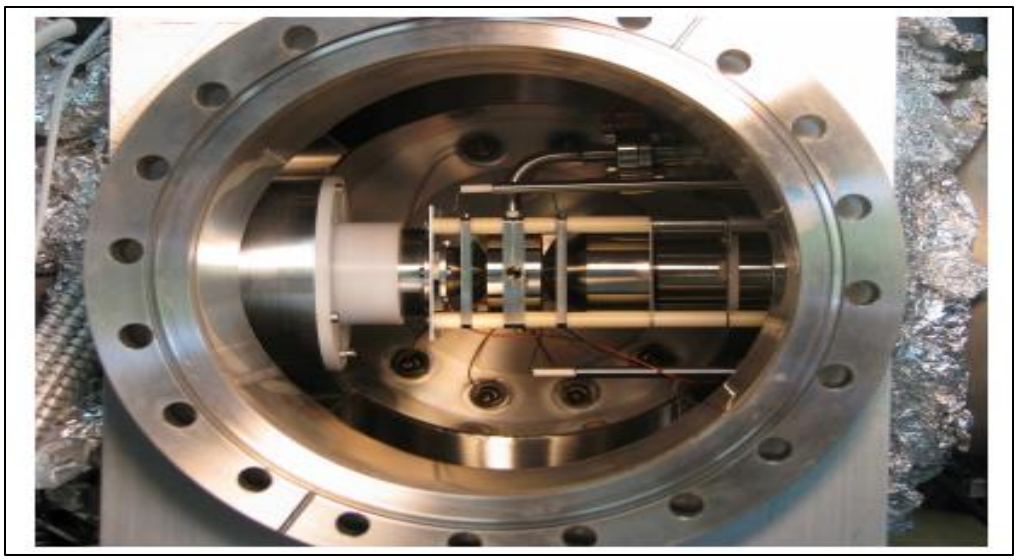

Figure 6: *Photograph of the 3D Paul trap opened*.

The trapped molecular ions are then exposed for up to several hundreds of ms to ~~the ion~~ or photon beam. The conditions are chosen such that a total of about 10% of the trapped protonated or deprotonated ions ~~were dissociated by collisions with the projectiles~~. We set this in order to avoid interaction of our molecule ions with more than one photons.

2.2.6 Time of Flight - TOF

In order to perform mass spectrometry of the content of the trap, the ions are extracted from the trap and accelerated towards a time–of–flight (TOF) tube.

The TOF is a large tube of known length which connects the Paultrap to a micro channel plate (MCP) detector. The molecular ions are sent through the TOF by an electric pulse which accelerate them to towards the MCP. The velocity of the ions depends on the mass-to-charge ratio of each ion.

The time that subsequently takes for each ion to reach a detector is measured. This time depends on the m/z ratio of the particle (heavier particles ~~reach~~ lower ~~speeds~~). From the time we can obtain the mass-to-charge ratio of the ions.

2.2.7 Micro Channel Plate Detector (MCP)

The micro–channel–plate detector (MCP) has a planar shape, chevron configuration and 50 mm diameter. The front plate is biased to -5 kV and the anode is kept at ground potential. The signal is read out by a 1 GHz digitizer for further analysis. When the extraction is completed, the RF of the ring electrode is switched on again and the DC voltage on the end caps is set to zero.

The complete operation process and the data recording process may be found in the Practical Manual Guide of the group.

2.3 Imaging Mass Spectrometry Technique - MALDI

Matrix-assisted laser desorption/ionization (MALDI) is a soft ionization technique used in mass spectrometry, which allows the analysis of biomolecules (such as DNA, proteins, peptides, sugars) and large organic molecules (such as polymers, dendrimers and other macromolecules), these molecules tend to be fragile and break when they are ionized by conventional ionization methods.[12].

The MALDI technique is quite similar to the electrospray ionization (ESI) technique. Both techniques are used for ~~the obtaining of the~~ ions of large molecules in the gas phase ~~via ionization process,~~ MALDI produces far fewer multiply charged ions.

MALDI techniques typically employ ~~the use of~~ Ultra violet lasers such as nitrogen lasers (337 nm) and frequency-tripled and quadrupled Nd:YAG lasers (355 nm and 266 nm respectively).

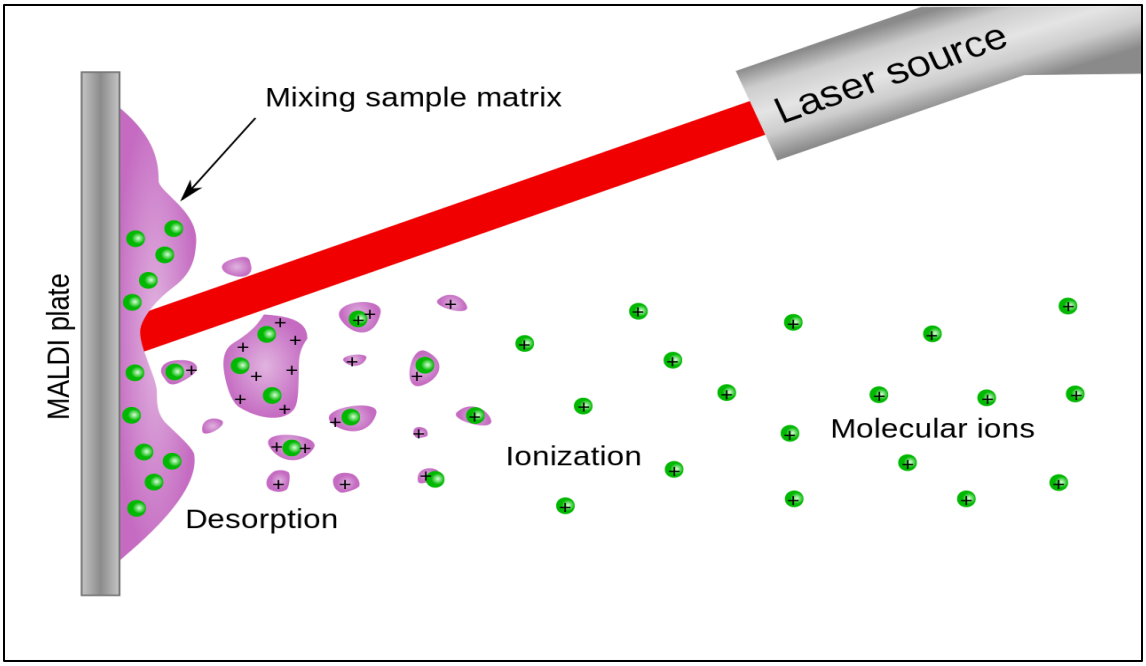

Figure 7: *Schematic draw of the MALDI technique*

The laser is ~~applied~~ to the matrix crystals in the dried-droplet spots. The matrix then absorbs the laser energy and the matrix is desorbed and ionized (by addition of a proton) by this interaction.

The heated mixture produced during the ablation contains many species: neutral and ionized matrix molecules, protonated and deprotonated matrix molecules, matrix clusters and nanodroplets. These species participate in the ionization of analyte.

The matrix then transfer protons to the analyte molecules (e.g., protein molecules), which charge the analyte. The observed ions after this process will be the initial neutral molecule [M] with ions added or removed in a similar way to ESI-MS~~.~~

~~We call this a quasimolecular ion,~~ for example $[M+H]^+$ in the case of a protonated ion, $[M+Na]^+$ in the case of an added sodium ion, or $[M-H]^-$ in the case of a deprotonated ion. MALDI is capable of creating singly charged ions or multiply charged ions ($[M+nH]^{n+}$) varying with the nature of the matrix, the laser intensity, and/or the voltage used.

Note, that mainly even-electron species, i.e. non-radicals are produced. Ion signals of radical cations (photoionized molecules) can be observed, e.g., in the case of matrix molecules and other organi c molecules. The type of a mass spectrometer used with MALDI during this work was TOF-MS (time-of-flight mass spectrometer), mainly due to its large mass range. The TOF measurement procedure fits well to the MALDI ionization process because the pulsed laser takes individual 'shots', similar to the electric pulses that send ions from the ion trap to the MCP detector in the ESI-MS technique.[12]

2.4 DNA

Deoxyribonucleic acid (DNA) is a macromolecule that carries most of the genetic instructions used during the growth, development, functioning and reproduction of all known living organisms and many viruses. DNA is a nucleic acid, one of the three major classes of biologically relevant molecules; alongside proteins and carbohydrates. Most DNA molecules consist of two biopolymer strands coiled around each other to form a double helix.

Each nucleotide is composed of a nitrogen-containing nucleobase, as well as a monosaccharide sugar called deoxyribose and a phosphate group. The nucleotides are joined to one another in a chain by covalent bonds between the sugar of one nucleotide and the phosphate of the next, resulting in an alternating sugar-phosphate backbone.

The nucleobases are classified into two types: the purines, adenine and guanine, being fused five- and six-membered heterocyclic compounds, and the pyrimidines, the six-membered rings cytosine and thymine. According to base pairing rules (A with T, and C with G), hydrogen bonds bind the nitrogenous bases of the two separate polynucleotide strands to form double-stranded DNA. When the hydrogen bonds are broken and the strands are separated, a new partner strand will follow the sequence of the old strand by a polymerase, results in two identically new DNA molecules, this is the process we know as DNA repairing.

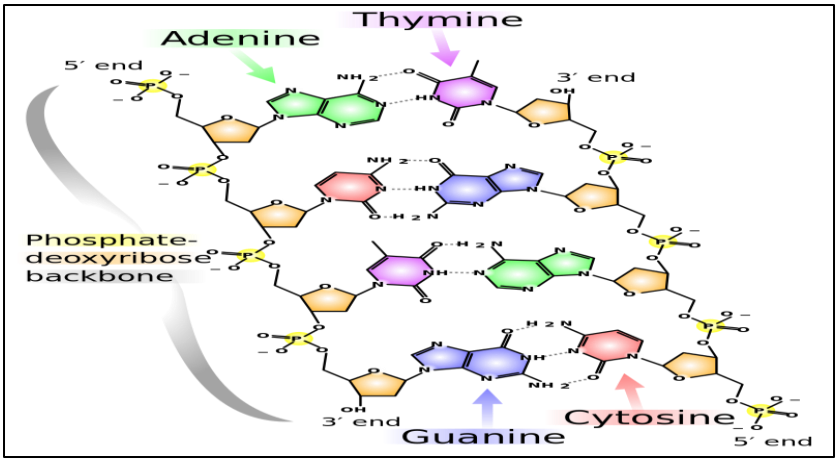

Figure 8: *DNA structure*[9]

2.5 BESSY

The storage ring BESSY II is a third generation synchrotron radiation source that provides 25% of the XUV–infrastructure in Europe [26]. Electrons are injected by a linear accelerator into the storage ring up to a maximal operational current of 300 mA and an energy of up to 1.72 GeV. The storage ring has a circumference of 240 m and contains a set of 11 permanent magnet undulators. These undulators provide ultrabright photon beams from the Terahertz to hard X-ray spectral range. A total of 50 beamlines are attached to undulators and dipole magnets and available to (external) users.

Figure 9: *The storage ring BESSY II (The Berliner Elektronenspeicherring-Gesellschaft für Synchrotronstrahlung m. b. H, Adlershof Berlin, Germany)*

3. Obtaining of small complexes of functionalized Ag_N:DNA

In order to study the X-ray induced damage to gas-phase DNA-NPs we need first to obtain molecular complexes formed by nanoparticles consisting of metal atoms (Gold, Silver) and a DNA strand.

Typically the ideal complex would be gold. Gold is used for many biological applications due to its non-reactive nature (non-toxic). For our approach we need to work with sufficiently light system~~.~~, to account for the limited mass resolution of the TOF system. However molecular complexes formed from the smallest gold NPs (undecagold Au_{11}) and DNA would have masses around 10 kDa and more. Furthermore the main problem is that the resonances for the gold inner shell excitation are above 1000and cannot be reached at the available soft x-ray beamlines at Bessy II. ~~.~~

On the other hand complexes based on silver are lighter and the resonance energies are below 1000 eV. Besides that, there are ~~some production technique already investigated~~ to obtain complexes formed from silver NPs and DNA.

In recent years there have been extensive efforts to realize ligand-stabilized metal nanoclusters composed of just a few tens of atoms of silver, corresponding to cluster sizes on the order of the Fermi wavelength (~ 0.5 nm in Ag and Au). This research on ligated, quantum-sized clusters is motivated by potential applications in chemistry, biology and materials science.

These applications all rely on the special sensitivity of fluorescence color and intensity to the specific base environment of silver clusters, which display wide-ranging peak emission wavelengths (400–800 nm) and quantum yields, depending on the oligonucleotide host[13][14].

A process for obtaining ~~of~~ Ag_N:DNA ~~is already established. We try to obtain such complex by~~ the purification method described by Shultz [15]. In particular we work with the complex refer to as Green1. This complex is formed by a double strand CGCCCCCCTTGGCGT and 11 atoms of silver. The compound has fluorescence emission peaking at 577 nm.

For the synthesis we employed High-performance liquid chromatography (HPLC) as main process~~,~~. More information about this technique in the Fundamentals part of this thesis. HPLC was combined with ESI-MS and MALDI for identification of the produced species. The latter step is important because distinct Ag_N:DNA complexes can have similar HPLC retention times.

4.1 Experiment

This experiments was performed at UMCG in the Department of Pharmaceutics.

As described previously, the protocol for synthesis consists of [15] two steps of HPLC purification to isolate the desired complex. We modified the process by using a different HPLC column.

Synthesis and structure of Strand 3:

To prepare the solution, DNA strands were used as received by DNA Technology, Denmark (standard desalting).Ag_N:DNA solutions were synthesized by mixing hydrated DNA (ammonium acetate buffer, pH 7) with AgNO3, followed by reducing with NaBH4. The Ag/DNA ratio was optimized for fluorescence brightness of our desired compound (21 atoms of Ag –DNA Dimer).

Strand	Sequence (5'-3')	DNA (µM)	NH_4OAc (mM)	$AgNO_3$ (µM)	$NaBH_4$
Green 1	CGCCCCCCTTGCGT	25	10	250	60

Table 1: *Recipe of the prepared solution which optimized the* fluorescence brightness of our desired compound (21 atoms of Ag – DNA Dimer)

Structure

It is well known that silver ions bind specifically to A, C and G bases at neutral pH. This enables non-Watson-Crick pairing by Ag^+ ions that simultaneously bind to two bases. Such Ag^+ pairing could occur between bases within a single strand, or as a bridge between two strands.

The previous studies of high resolution mass spectrometry (MS) to study the composition of these pure solutions [15] have shown a variety of charge states with different numbers of Ag atoms formed.

The study suggests an overall Ag:DNA structure with a neutral, rod-like chain of silver atoms surrounded by a base-bonded Ag^+ frame. In agreement with this picture, the peak absorbance energies decrease with the number of free electrons which agrees with the recent calculations done for silver nanocluster rods. [18]

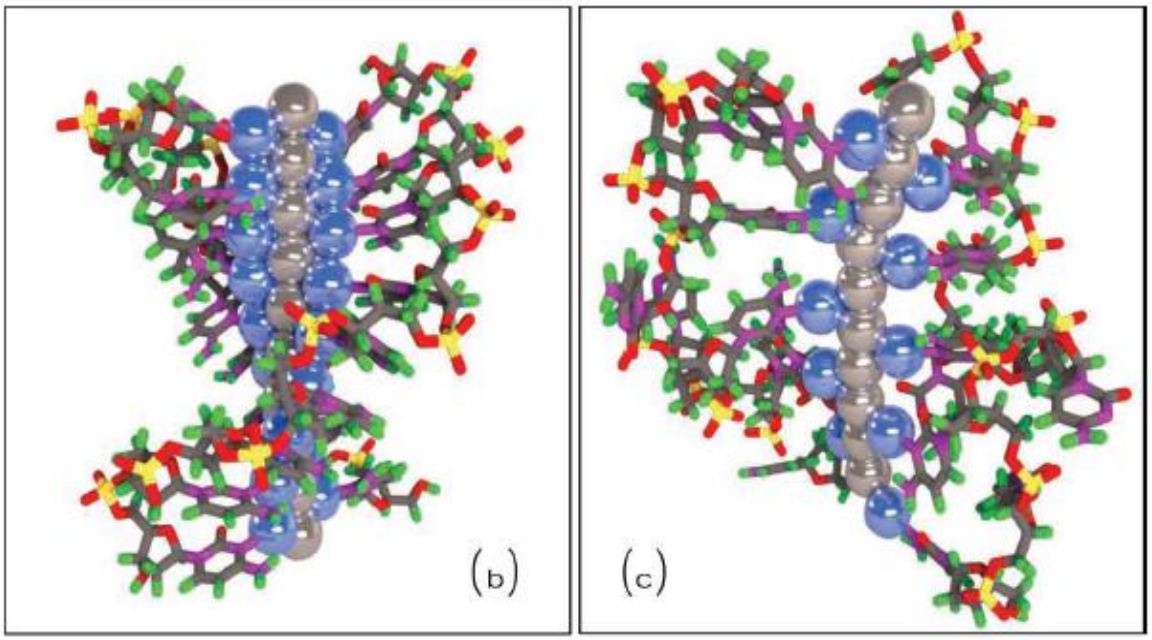

Figure 10: *Examples of the corresponding structures. Rod-like, neutral clusters (gray) are shown attached to DNA bases via peripheral Ag + (blue), in repeat tetramer (b) and trimmer (c) units. For simplicity, all bases are shown as C, but could just as well be A or G since these bases also contain conjugated ring nitrogens.*

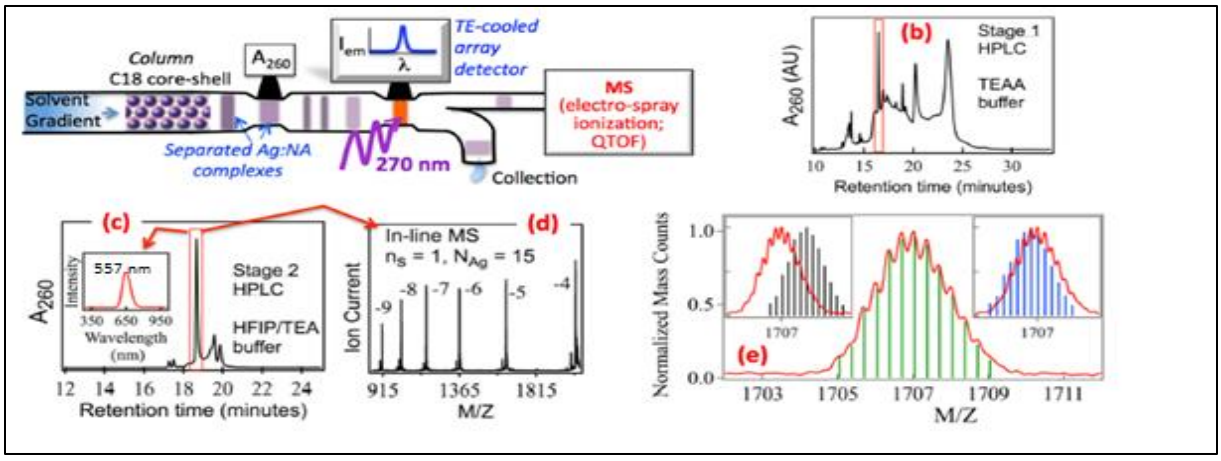

Figure 11: *Schematic of HPLC-mass Spectrometry method to obtain Ag_N:DNA complexes, in particular for a complex with characterized wavelength of 557 nm.* [15]

HPLC Stages

DNA prepared solutions typically contain a mix of dark and bright (fluorescent) compounds of DNA-Silver that ~~will~~ depend on the different combinations of Ag atoms and number of Strand.

In *Figure 11* the procedure is sketched.

1. The solution containing different Ag_N:DNA complexes~~,~~ is synthesized following the recipe from [16].
2. The prepared mixture is pushed into the HPLC system where we run the first stage. Mobile solutions are given in the recipe. In the first stage of HPLC we separate and collect the fraction of the mixture which emits in the characterized wavelength of the complex we want to isolate (557 nm) (b). We use the absorbance wavelength 260 nm as guide to know when an Ag_N:DNA complex is going through the detector and we collect during the retention time at which we also detect fluorescence at 557 nm.
3. Different complexes often have identical retention times. In case in the first stage we have collected more than the desired complex, for that reason the collected fraction is again pushed into the HPLC and we run the second stage. The second stage has different mobile solutions which are also given in the recipe. Again we separate and collect the fraction of the mixture which emits in the characterized wavelength of the complex we want to isolate (c).
4. After this two HPLC stage we proceed immediately to check and identify the collected solution using high resolution mass spectrometry or MALDI technique (d), (e).

It is important to be able to identify a single complex, only in the fraction we collect after the second stage. Otherwise no full isolated of the require complex was accomplished.

4.2 Results and Discussion

Purification and isolation (HPLC)

HPLC runs used a Waters 2695 Separations Module with auto-injector and a Waters 2487 Dual Wavelength absorbance detector (10 µL volume), set to monitor 260nm. Pre-concentrated samples were injected in 100 - 200 µL volumes into a C4 column: 150x4.6mm column with 5µm particle size and 300Å pore size (Phenomenex). All samples were run at room temperature at 1mL/min.

First Stage

Mobile Phase: 35 mM triethylammoniumacetate (TEAA), water and methanol (pH 7).

Solvents "A" and "B" were prepared by diluting the stock solution to 35mM TEAA in water for the "A" component; and in MeOH for the "B" component.

This initial purification of Ag_N:dDNA is 1% per minute with linear methanol gradients starting at 5%. The final methanol concentration was 50%. Each gradient was preceded by 10 minutes of equilibration at 5% methanol, and followed by 10 minutes at 95% methanol.

The spectrum obtained after this first stage of HPLC is shown in figure 12:

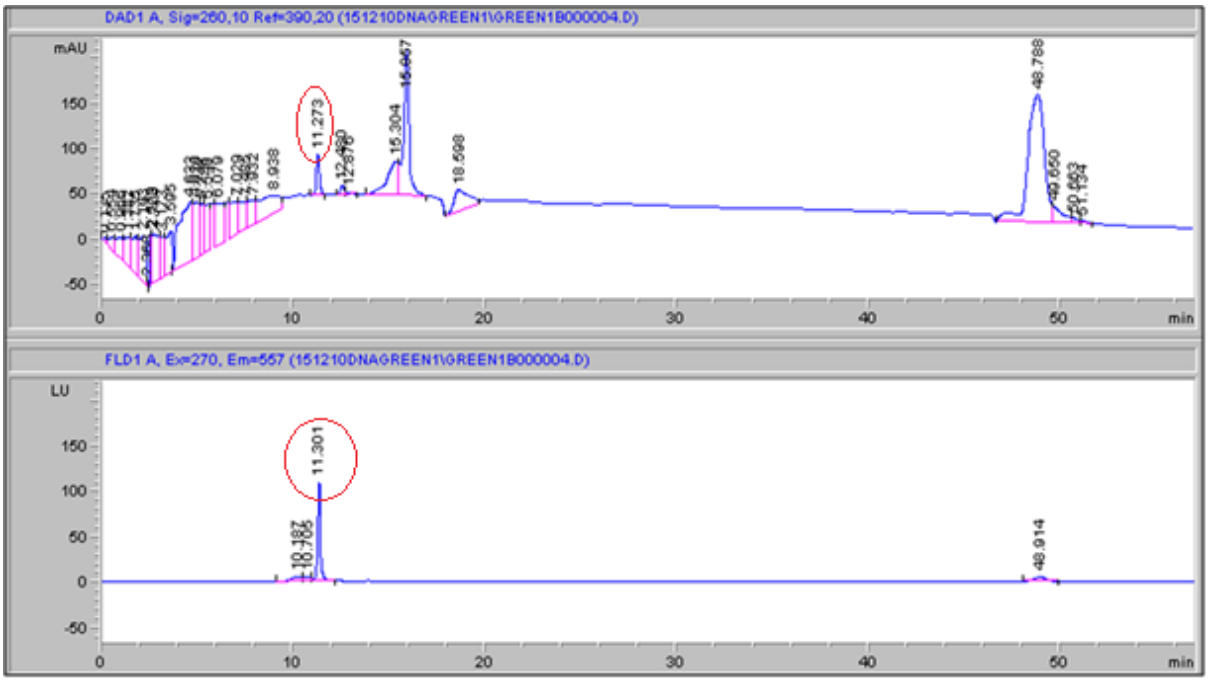

Figure 12: *Retention times for different AgN:DNA complexes in the prepared solution. The peaks for 260 nm indicates when a complex is going through the detector/column. The peak for 557 nm indicates when the specific complex with such characterized emission wavelength is going through the detector/column, in this cases Green1.*

As stated in the Fundamental part different compounds have different retentions times, and this is precisely what we see here. The first spectrum shows data for an absorbance wavelength of 260nm which is a common feature for DNA compounds. ~~The different peaks that we observed in the top spectra are due to different retention times at which we have a DNA compound going through the detector.~~

The second spectrum displays fluorescence at a wavelength 557 nm, which is the specific fluorescence of the compound we want to isolate. (Green1 formed by a DNA dimer and 21 atoms of Ag).

We then collected a 1 ml fraction containing the material related to the peak at the Excitation/Emission wavelength of Ag_{21} Green 1 dimer according to literature, which is found at ~~:~~ 11.2 minutes. This sample we have collected ~~it is supposed~~ contains the specific complex Green1, but as we explained before, different compound may have different retention times.

To isolate the desired complex from the mixture obtained after the first HPLC run, a second HPLC run is needed. In the work of Schultz et al. it is stated that after the first stage there are still two compounds present and that a second stage is needed to remove the dark (non-fluorescent) complex and keep the desired bright (fluorescent) complex.

However, in this work a different column type was used, so the conditions ~~are~~ not identical. It is possible, that only the bright complex ~~is~~ present after the first run, but it also possible that more than one dark compound ~~are~~ present. To be sure of the complex we have collected, we try to use both, MALDI and ESI-MS to identify them.

~~During the experiment the used column is different to the one used in [15] so it may contain only the bright one or even more than one dark compound. To be sure of the complex we have collected, we try to use both, MALDI and ESI-MS technique to identify them.~~

Identification (MALDI)

After the fraction collection we tried to identify the compounds we collected by means MALDI.

To this end we prepared a Matrix solution as follows: Saturated 3-HPA (Hydroxypicolinic acid) in 50% Acetonitrile with 0.1% TFA (TriFluorAcetic acid) was mixed with 10mg Diammonium hydrogen citrate/ml. Then we pipet 0.5µl matrix solution onto each spot and allow it to dry. Finally we pipet 0.5µl sample onto each matrix spot and allow to dry.

We proceeded to measure spots at 75, 25, 10, 1 and 0.2 µM in 30mM NH_4Ac buffer pH 7 in negative and positive mode. To increase the concentration we used a Zip tip concentration procedure. (Details in the Annex)

Both modes showed similar results and we got clear response only at 10 and 25µM concentration levels, indicating that the 1µM and 0.2µM concentration was insufficient for use with the MALDI technique.

To know at which masses the expected Ag_n/DNA complexes appear in the mass spectrum, we have to take into account the structure of these complexes. The silver cations are attached to the neutral silver and at the same time they subtitude one of the hydrogen atoms of the DNA.

As we stated previously the structure is formed by a neutral rod-like chain of silver atoms surrounded by a base-bonded Ag^+ frame. In agreement with this picture, the peak absorbance energies decrease with the number of free electrons. Previous Studies calculated the relationship between the total number of atoms in complex and the numhber of neutral and cation silver in the complex.

For our specific strand the number of cations in the structure is 9, so there is a core rod of 12 neutral atoms of silver.The length of this free electron system(neutral rod) is the primary source of Ag:DNA color[14].

In the case of the MALDI technique there are therefore a number of specific masses, which have to be investigated. In order to order to identify the complex, we display the masses in the *table 2*.

	Terminal	OH/OH	Phos/OH	OH/cycl Phos
DNA Monomer	4480,9	4478,757	4558,72	4540,71
DNA Dimer	8961,8	8957,514	9117,44	9081,42
21 Ag Atoms	2245,005	2245,005	2245,00	2245,00
21 Atoms Ag + DNA Monomer	6725,905	6711,762	6803,72	6785,71
Green 1(21 atoms Ag + DNA Dimer)	11206,80	11190,519	11362,4	11326,4

Table 2: *Relevant masses of the complex Green1*

The column 3, 4 and 5 show the masses of the molecular complex with a phosphate group, hydroxide group or cyclic phosphates group attached to its end.

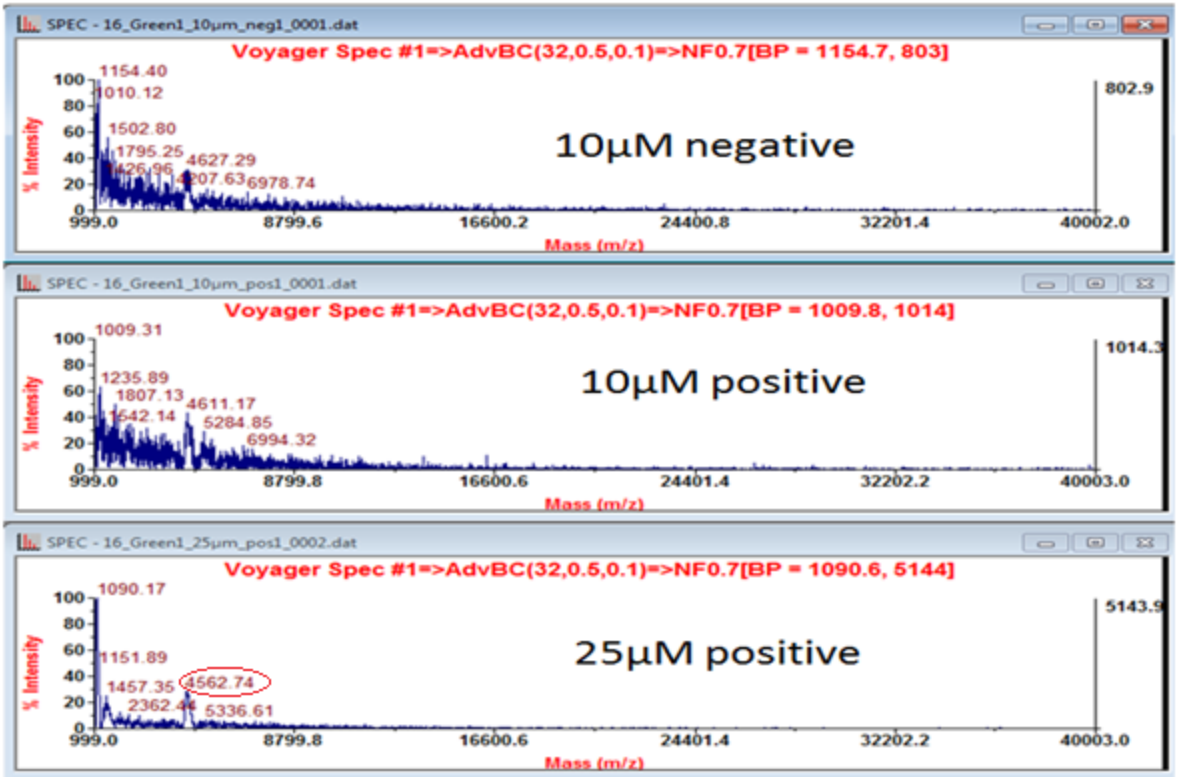

Figure 13: *Mass spectrum by MALDI of the collected fraction for different concentrations. Due to imperfect calibration masses are shifted.*

Clearly, for all concentrations under study in positive and negative mode, the collected fraction seems not to contain any silver stabilized DNA. An explanation could be ~~and~~ insufficiently low concentration. The single strand (without silver) on the other hand, could be identified in this fraction, after enrichment. Due to the laser desorption, MALDI is not the gentlest technique possible. It is feasible that the observed bare DNA strand has lost the attached silver during the MALDI ionization/desorption process.

Also due the aggressive evaporation process the bonds between DNA and silver may be broken leading to just DNA strands and losing in the process the complexes we synthetized. Thys is why an additional ionization technique was investigate.

Identification (ESI-MS)

MALDI with the chosen matrix seems to not be sensitive enough so we decided to use ESI-MS instead. The TEAA present in the collection fraction was removed using the speedvac technique (see Annex). The sample was also concentrated by resuspending it in a smaller volume.

The enriched sample was then flow injected into the ESI-MS to identify the Ag_N:DNA complexes present.

The overall charge of the electrosprayed Ag:DNA complex, expected in the mass spectrum is:

$$-eZ = -en_{pr} + Q_{cl}$$

Where n_{pr} is the number of protons removed from the DNA and Q_{cl} the charge of the silver cluster which is given by the number of ~~cation~~ silver in the structure (Figure 19). Higher values of Q_{cl} imply more protons removed to reach a negative ion charge.

The mass of the ionized Ag:DNA is given by:

$$M = M_{DNA} + m_{Ag}N_{Ag} - (Z + \frac{Q_{cl}}{e})$$

M_{DNA} is the mass of the DNA strands in the complex, and $Z + \frac{Q_{cl}}{e}$ the mass of the protons removed from DNA to achieve the $-eZ$ charge. We use this relation to identify the silver cluster charge from the Q_{cl}-dependent shift that we find in the ESI-MS spectra..

$$\Delta\left(\frac{M}{Z}\right) = -\frac{Q_{cl}}{e}$$

The identification by ESI-MS get the same results ~~than~~ for MALDI technique, for higher concentration of the collected fraction we could identify the strand without any atom ~~silver~~ but we could not see any complex

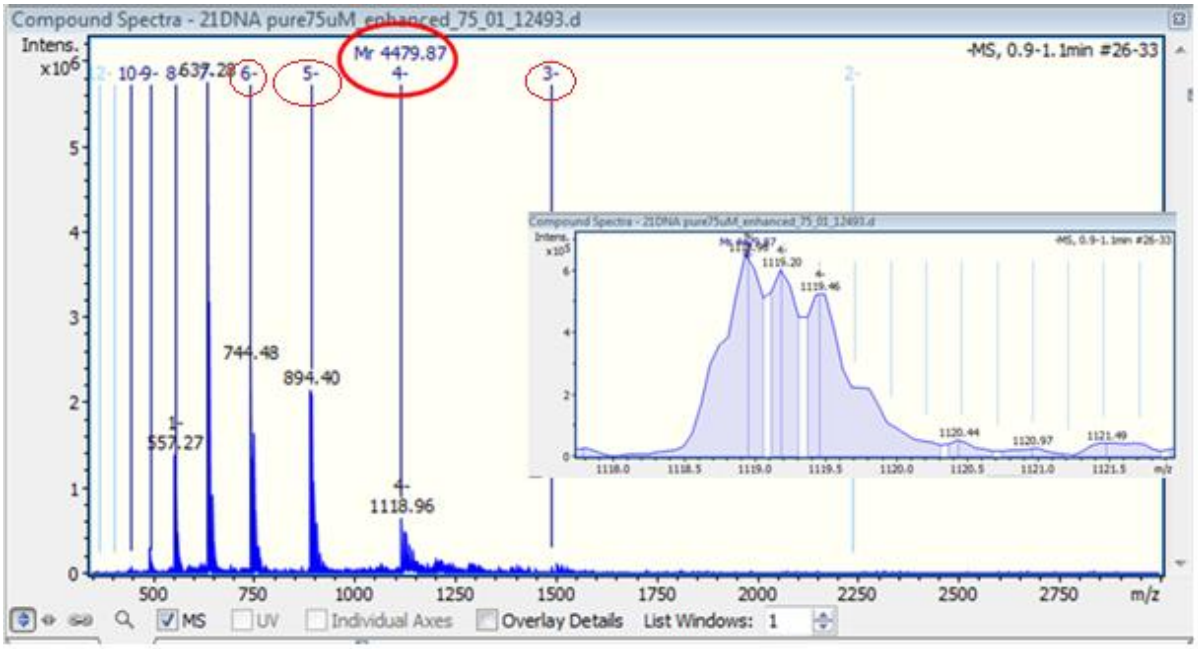

Figure 14: *Mass spectrum by ESI-MS of the collected fraction for 25µM.*

4. DNA Fragmentation

Pioneering study on DNA strands fragmentation has been carried out by our group in the past, in his thesis Olmo González Magaña studied the fragmentation of the single stranded oligonucleotide GCAT [9]. During these experiments electrospray ionization was used to bring these species into the gas-phase in doubly protonated form for exposure to soft X-rays.

We have continued working from that point; first studying the fragmentation of GCAT, which can be found in the annex. Subsequently studied the fragmentation of a more complex strand of DNA, the one we call *Strand3* (TTAGGGCCGCCG).

For the study of GCAT fragmentation existing data was compared to the data obtained in this work. In both cases the positive ion electrospray ionization mode was use, i.e. doubly protonated $[GCAT+2H]^{2+}$ was used. For the study of the complex strand we have carried out the experiments mainly in negative mode, where DNA strands tend to be more stable.

3.1 Experiment

The experiments based on photoionization that we present in this chapter have been carried out at the synchrotron beamline BESSY II U49/2-PGM1 (Berlin, Germany)

Our home-built electrospray ionization source (Paultje) was used to spray a 40µM solution of the oligonucleotides (dGCAT, Strand3) solvated in a prepared mixture. More information on the solution composition are provided in the Annex. The ESI beam was send to the 3D RF-ion trap via ion funnel, octupole guide and quadrupole mass filter and then accumulated to reach sufficient target density (more information about this process can be found in Fundamentals).

Strand3 is an oligonucleotide 12 nucleobases long (TTAGGGCCGCCG). We study its fragmentations for 5 specifically chosen energies in the range of 90-540 eV.

The typical operating conditions of the experiment are shown in the following table

Exposure time	0.4 - 0.5 seconds
RF filled	1 – 1.1 seconds
Number Density of the target	10^8 cm^3
Pressure of 3D Trap	10^{-8} mbar
Losses Rate	10%
Beam Intensity	300 µA

Table 3: *Operation conditions*

For the collisional cooling of the protonated/deprotonated oligonucleotides we applied a He buffer gas pulse. Then the target was exposed to monochromatic soft X-rays at a number of different energies. After the beam exposure, the cations were extracted into a linear time-of-flight (TOF) mass spectrometer and detected using a multichannel detector [7].

3.2 Results

For the photoionization and photo fragmentation of Strand 3, mass spectra were recorded at several energies, ranging from 90 eV to 540 eV, to cover N, O and C ionization and resonance energies (the explanation for the chosen energies can be found in *table 4)*.

~~Our studies were mainly focused on the fragmentation of deprotonated oligonucleotides in negative mode, where DNA stability is higher.~~

Photon Energy	Explanation
296 eV	C 1s ionization energy
532 eV	O 1s excitation energy
540 eV	O 1s ionization energy
400 eV	N 1s excitation energy

Table 4: *Energies studied*

It is crucial to recall, that we set the exposure time in order to obtain a 10% loss for the parent peak, in other words we ensure that not more than 10% of the trapped photoionized oligonucleotides underwent more than one absorption process.

The results have shown that the first important observation is the much lower yield of fragment ions and ions formed by non-dissociative ionization, as compared with experiments carried out in positive mode with $[GCAT+2H]^{2+\cdot}$. A large fraction of absorption processes clearly does not show up as negative ions. This is clearly obvious from the spectrum in the next figure.

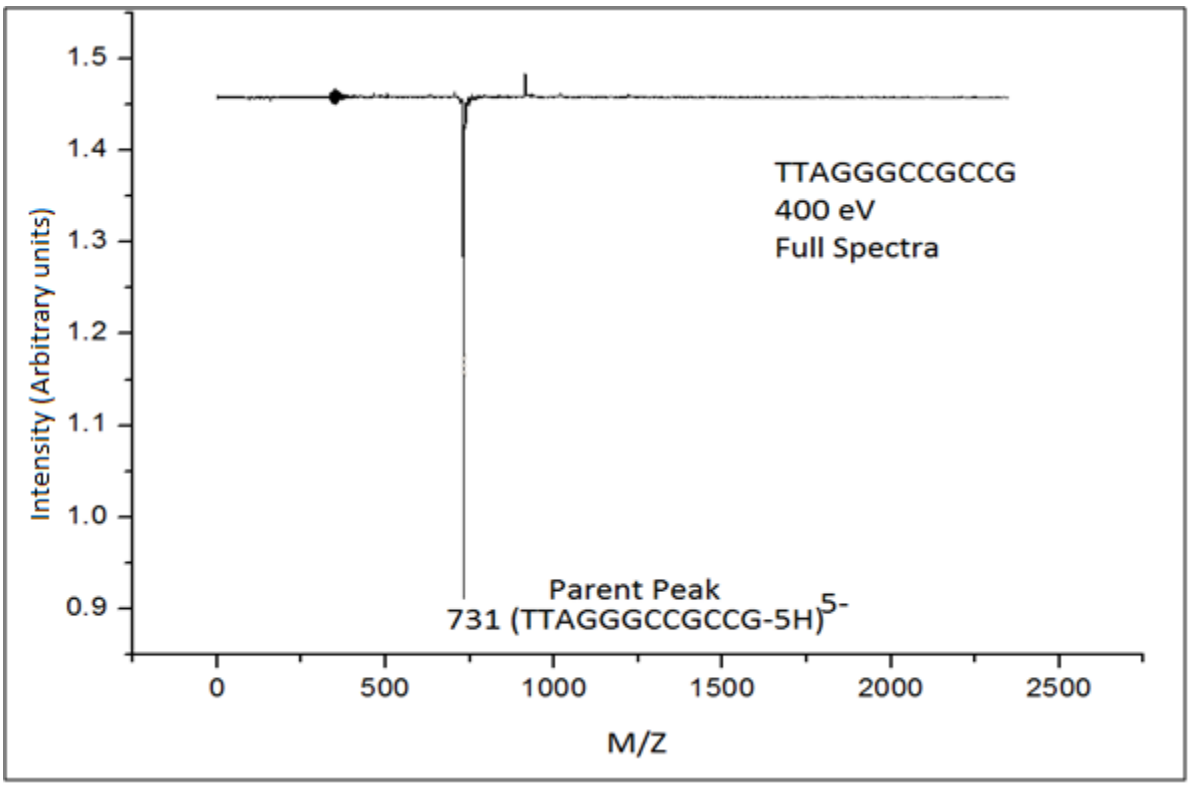

Figure 15: *Mass Spectrum of the* $[TTAGGGCCGCCG-5H]^{5-}$ *after 400 eV photons absorption. The loss of parent ions manifests as a negative peak.*

In *figure 15* the net effect of 400 eV photon absorption by [TTAGGGCCGCCG-5H]$^{5-}$ is shown. The negative peak indicates the losses in the parent peak due to the photoabsorption and was experimentally set to be 10% of the initial intensity peak. The fragments and ionization peaks ~~appears as positive~~, the ~~main~~ peak is the ionization peak [TTAGGGCCGCCG-5H]$^{4-}$.

Most likely, X-~~R~~ay absorption ~~leads to~~ detachment of several electrons, as in a negatively charged ion the extra electrons are typically only weakly bound. If there is not too much negative charge, it is feasible that the core excitation or ionization, deposits enough energy to detach all these electrons, leading to formation of neutral or even positive ions, both unobserved in the negative mode spectra.

From the measured mass spectra for different photons energies, we obtained the relative total yield found as a function of the photon energy (eV) by integration of the negative parent peak. The data we obtained are relative taking into account an unknown number of ion in trap, trap dimensions and other absolute parameters.

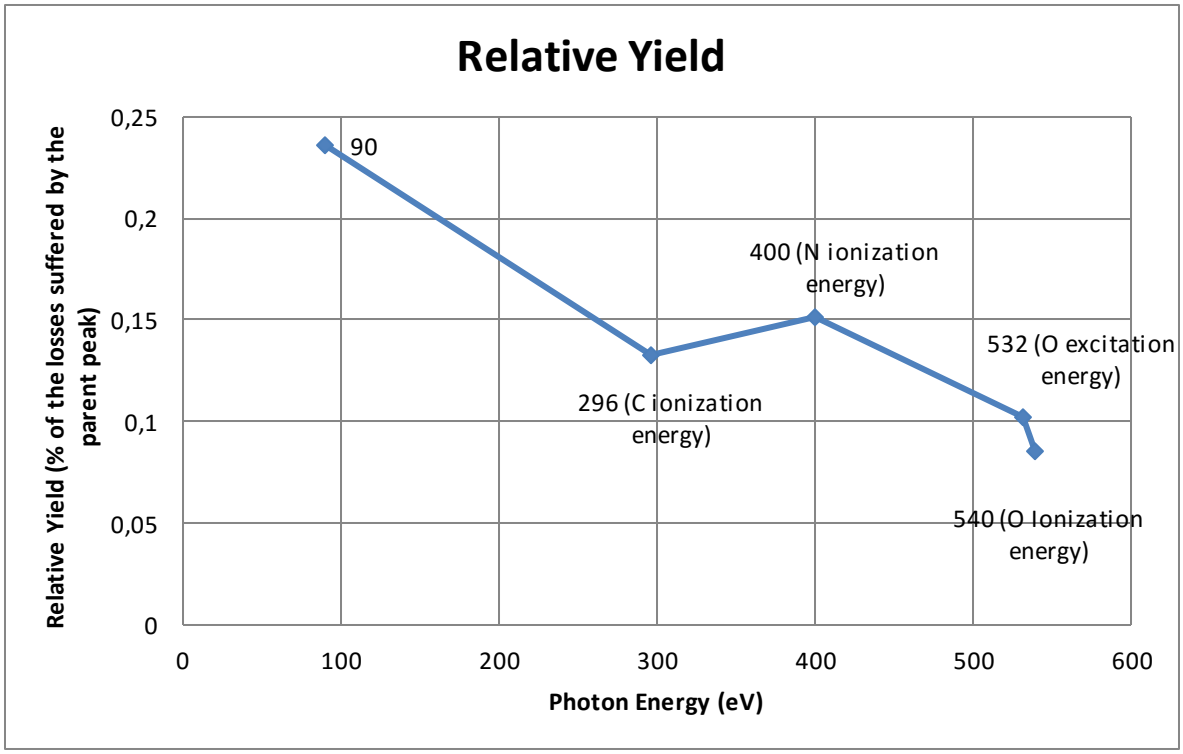

Figure 16: *Relative Yield of the strand3 five times negative ionized [TTAGGGCCGCCG-5H]$^{5-}$ for different energies.*

It is obvious that the maximum yield appears to be for 90 eV, finding in line with the expectations, the photoabsorption cross section for DNA is commonly larger at this energy [9].

In the spectrum (figure 15) there are two different classes of peaks: the peaks as a result of fragmentation and the peaks due to ionization. We determine the contribution of each of these peaks in *figure 16* where we split the contribution in the ~~Relative Ionization Yield, and the Relative Fragmentation Yield.~~

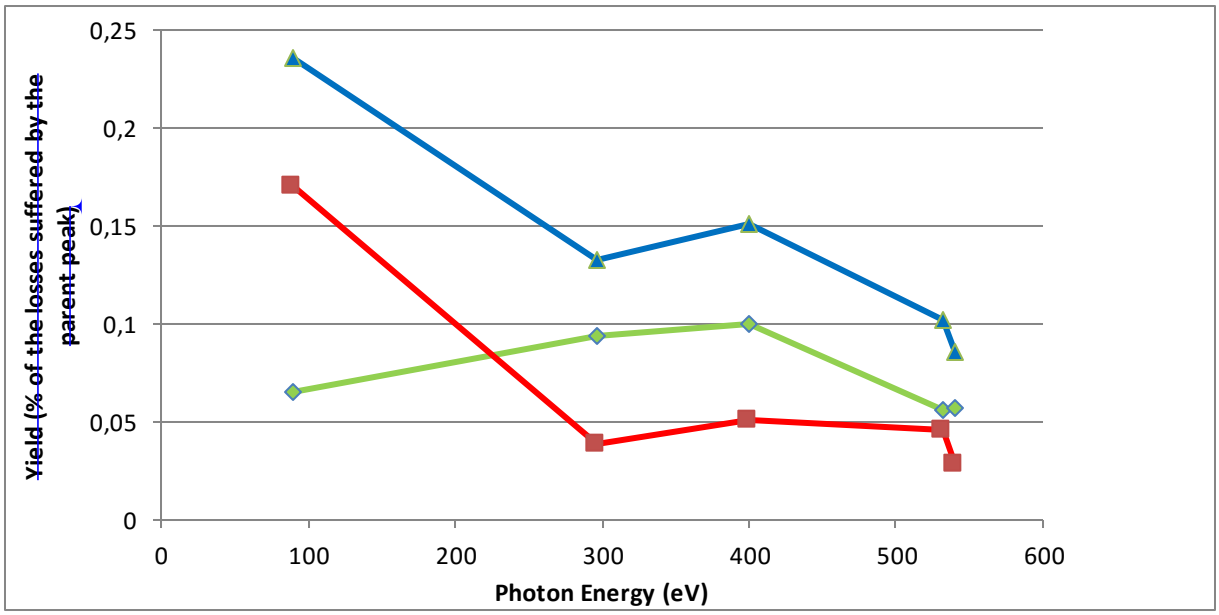

Figure 17: *Relative ionization yield (RED) and fragmentation Yield (GREEN) of the five-fold deprotonated strand [TTAGGGCCGCCG-5H]$^{5-}$ for different photon energies.*

The *figure 17* provides us with valuable information. Clearly indicating that the high relative yield for 90eV is mainly due the really high ionization yield while the relative fragmentation yields remains similar to other energies (or even less for some of the energies, 540 eV).

There are two processes mainly occurring during the interaction between the x-ray photons and the DNA strand i) inner shell photoionization and ii) de-excitation via and Auger process.

In photoionization process at 90 eV , inner shells are inaccessible and the photon removes one of the molecular valence electrons (C, N, O) which leaves the strand with one negative charge less (see figure 18) . This process does not deposit a large amount of energy into the system. For this reason we can see in *figure 9* that for 90 eV ionization cross sections are high whereas fragmentation cross sections are low[-].

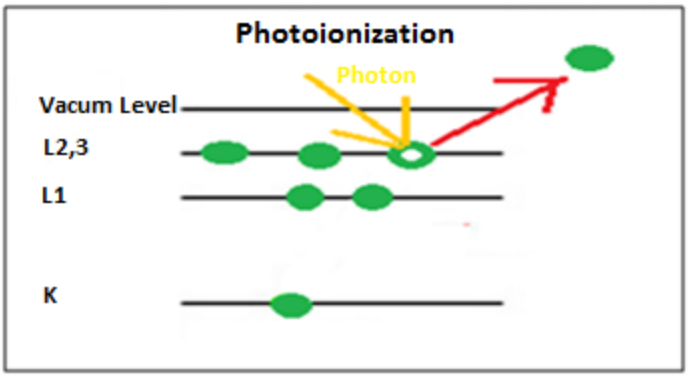

Figure 18 Photoionization process*: The energetic photon remove one valence electron from the atom, leaving the atom positive charged.*

For higher energies the predominant process is and inner shell excitation/ionization followed by an Auger process (*figure 19*). In the *table 4* we showed that the energies were chosen to be at a strong resonance for 1s excitation in C, N and O, as well as slightly above ionization threshold for the three elements. These more energetic photons have enough energy to remove the 1s electron from the atom. Once a 1s electron is removed (or excited), the atom suffers an Auger process. (Displayed in figure 19).

In the Auger process two or more electrons are involved (Auger Cascade). This increases the deposited energy into the system. The fragmentation of the strand depends on the deposited energy, for that reason in *figure 12* we see how the fragmentation increases for the higher energies (Auger process is predominant for such energies).

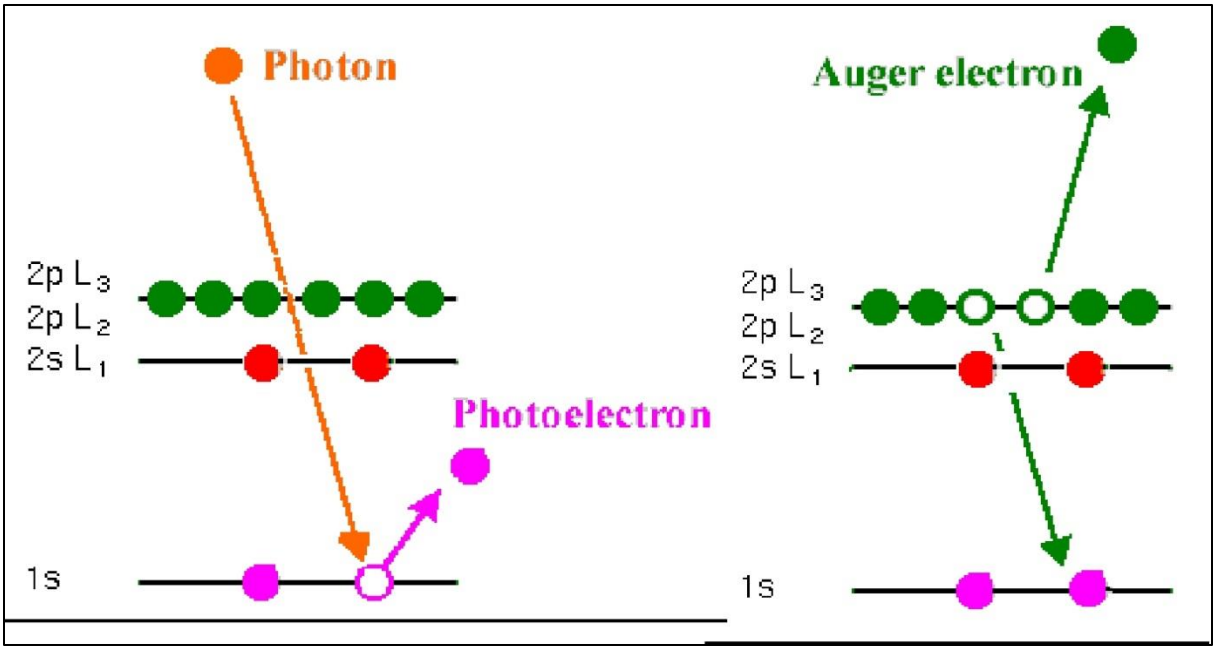

***Figure 19 Auger process**: The energetic photon removes a 1s electron from the atom. An electron from a higher energy level de-excites into the vacancy and the energy is transferred to another electron, which is ejected from the atom.*

Both, fragmentation cross section and ionization cross seems to have the same pattern from which we try to obtain some explanations in the discussion part.

After comparing the general picture we get from the spectras, we can now get into the details. For that purpose we show below a zoom into the fragment region for 400 eV photons. The main peaks can be identified. (400 eV shows the richest fragmentation pattern)

The notation chosen was established by Mcluckey and it will allow us to get some conclusion easier. There will be a, b, c, d fragments (fragments broken from the 5'terminal (left)) and w, x, y, z fragments (fragments broken from the 3'terminal (right)). It is easy to understand if we check the example sketched in figure 20.

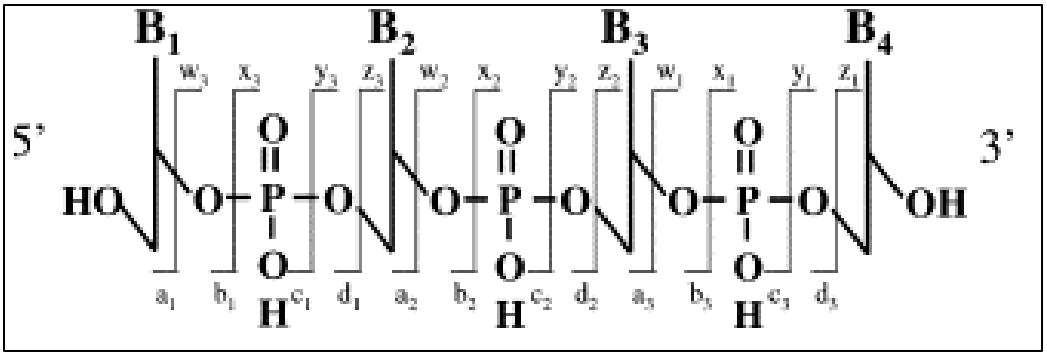

Figure 20: *Schematic explanation of the Mcluckey notation*

Now let see the peaks we found for one of the photon energies from the table 4 (540 eV). The parent peak is ~~the strand five time deprotonated~~ (TTAGGGCCGCCG-5H) $^{5-}$ = (M-5H) $^{5-}$ with mass equal to 731.5 Da.

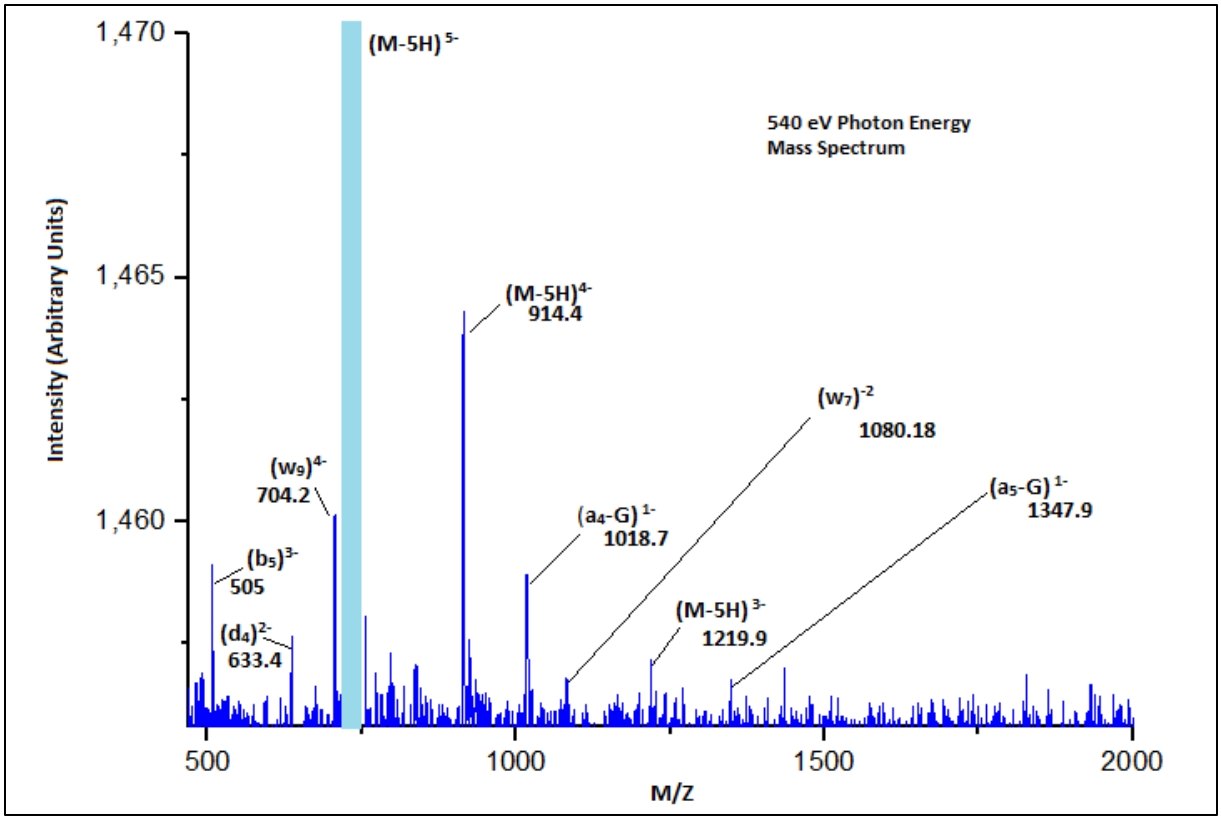

Figure 21: *Mass spectrum of the interaction products of 540 eV photons interacting with the strand TTAGGGCCGCCG*

The main peak is due to non-dissociative electron detachment into (M-5H) $^{4-}$. Furthermore there is a series of fragmentation peaks due sequences of different nucleobases length.

~~The peaks are due~~ to a_4 and a_5 accompanied by base loss (G) in different charge states, and ~~there is~~ b_5 and d_4 fragments~~,~~ furthermore there is ~~one~~ w_9, which implies a break between A and G~~, and w_7~~. All these fragments ~~come~~ from breaks in the GGG region as ~~we~~ sketch in figure 22.

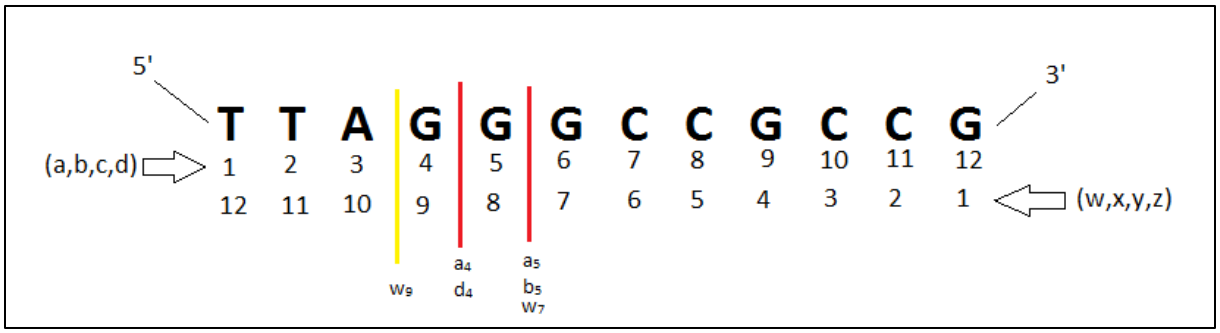

Figure 22: *Strand sketch of the break points found in the fragmentation pattern for ~~the interaction between the strand3 and 540 eV Photons~~*

~~This may~~ be an important finding, but first we want to know if there ~~is~~ different outcomes for different energies. To this end we compare, in figure 23, 24 and 25, the mass spectr~~um~~ of the interaction product for different energies. (296 eV, 400 eV, 532 eV)

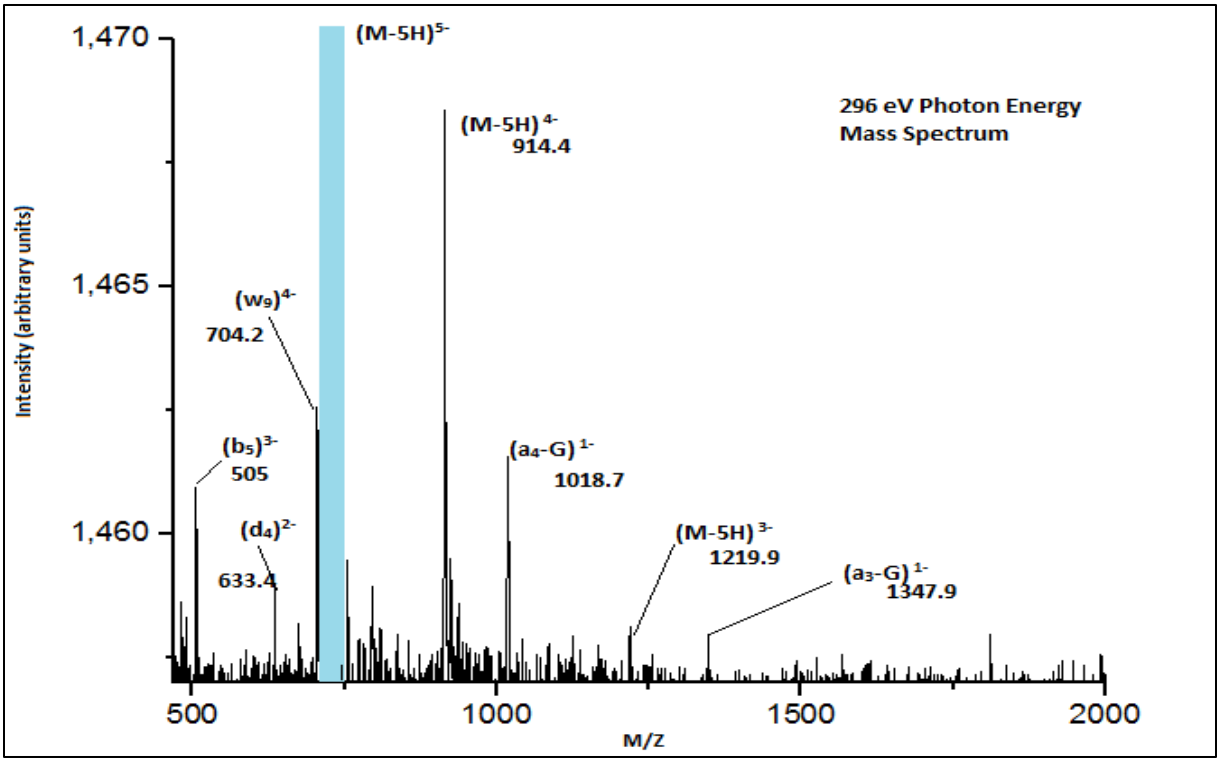

Figure 23: *Mass spectrum of the interaction products of 296 eV photons interacting with the strand TTAGGGCCGCCG*

As we can see in both figures, for ~~the all~~ energies ~~the product pattern we obtain after expose our strand3 five times deprotonated to soft x-ray is similar~~. ~~The fragmentation peaks identified for 540 eV appears again, with more or less relative intensity.~~

The main different seems to be the presence of more small unidentified peaks for smaller energies and also a higher relative intensity of the ionization peaks.

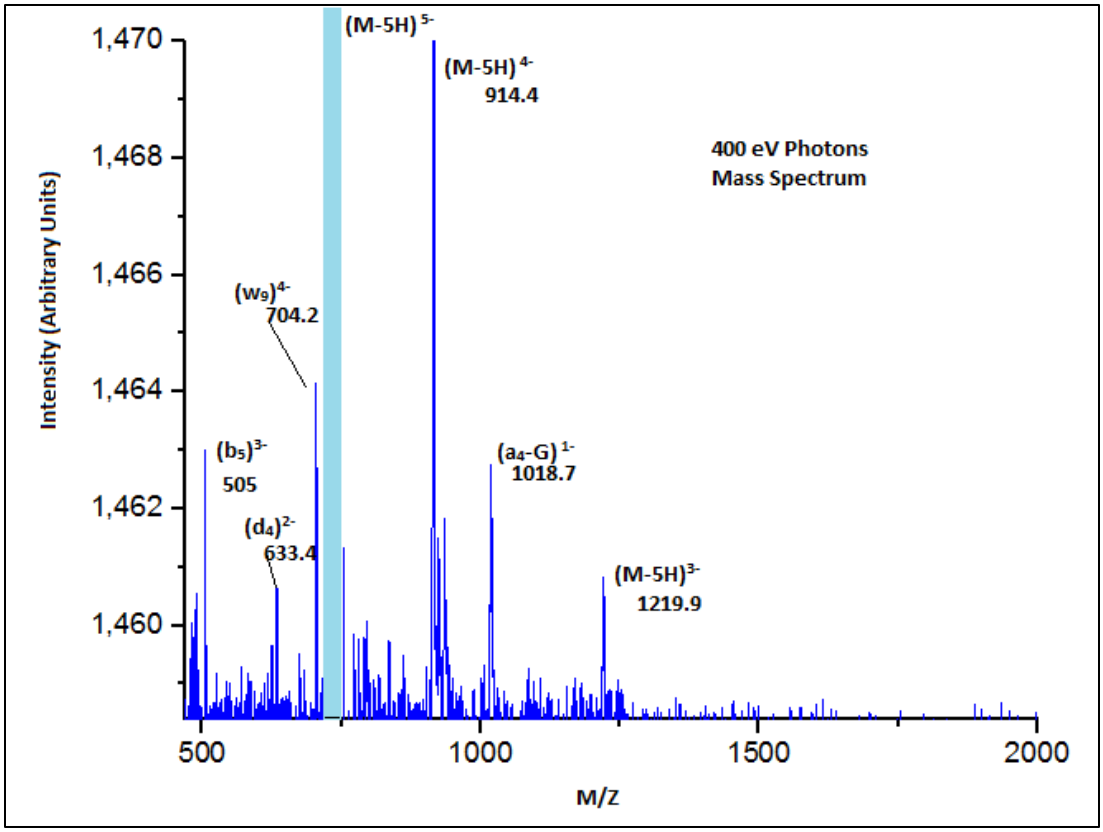

Figure 24: *Mass spectrum of the interaction products of 400 eV photons interacting with the strand TTAGGGCCGCCG*

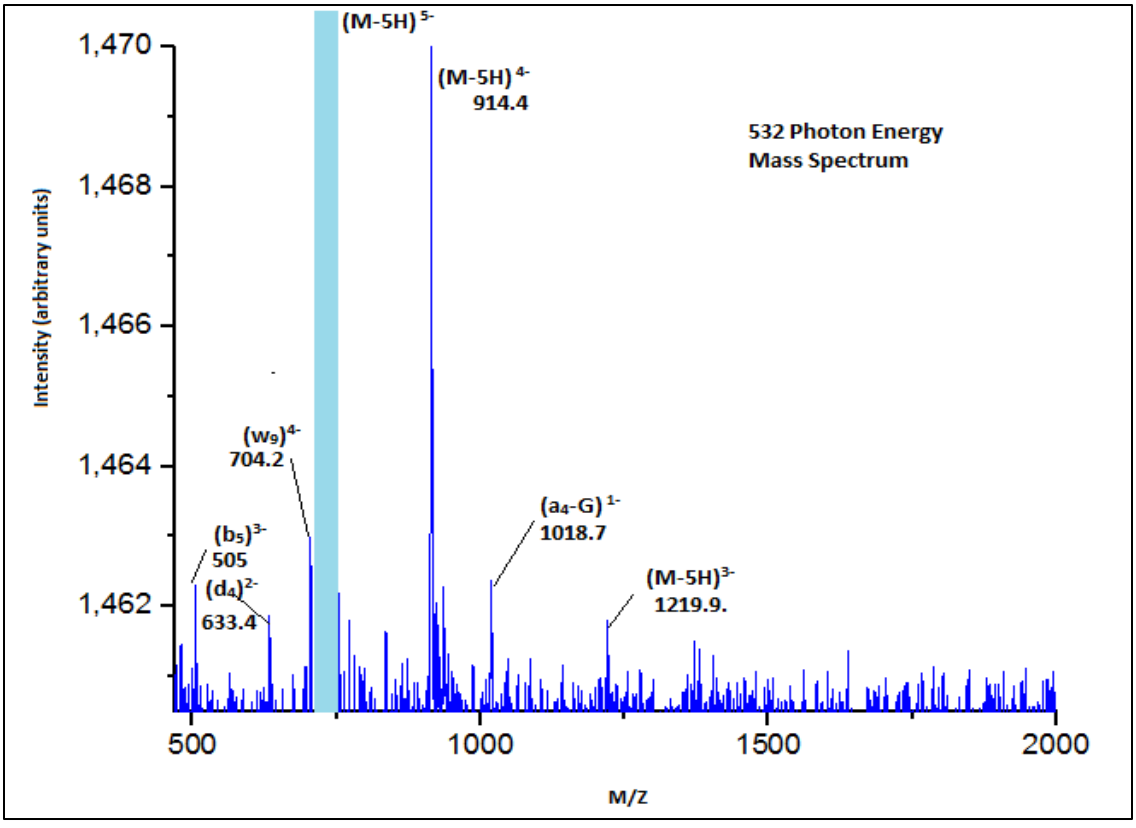

Figure 25: *Mass spectrum of the interaction products of 532 eV photons interacting with the strand TTAGGGCCGCCG*

We can obtain some preliminary information before getting into the details. There are more fragments for the intermediate energies (296 eV and 400 eV) than for the highest ones and the lowest one. There are two possible explanation for this, first the lowest energy (90 eV) induces some fragmentation but mainly ionization (15.5% relative intensity for the main ionization peak (TTAGGGCCGCCG-4H) $^{4+}$), and second, for higher energies (532 eV and 540 eV) the fragments loose many electrons leaving the oligonucleotide neutral or positive so we can´t detected them. Also if we focus only on the ionization peaks we observe how their relative intensities follow the same pattern, this pattern for the relative intensities is not the same for intensities of the fragmentation peaks, whose pattern may seem random.

3.3 Discussion

In this section we try to interpret the data from the previous section based on the structure of the oligonucleotide under study, [TTAGGGCCGCCG-5H] $^{5-}$. There most interesting findings is the fragmentation pattern. If we look again the mass spectrum we obtained. We can clearly see that all the fragments come from a break bond involving guanine (G) or adenine (A) nucleobase. This is not surprising.

Previous studies [23] have shown that the electron hole (radical cation) migration in DNA is possible and, in fact, occurs over a long molecular distance. These studies also suggest that the DNA contains sacrificial sites, particularly sites comprising guanine (G) rich sequences that are positioned optimally to absorb holes. Thus, G-telomeres found at the end of chromosomes have been proposed as candidates for "genome protectors". In particular, in humans, these telomeres consist of tracks of TTAGGG sequence, which is, and non by accident, part of our strand.

After an excitation process occurring in the DNA (such an Auger process induced by soft x-ray radiation) the generated holes migrate through the DNA molecule until they reach the guanine (G) nucleobases. For that reason, it is not surprising that most of the fragments appears to come from a guanine (G) bond broken, which is the localization in the strand where the excitation (holes) migrates to.

Therefore, this explains why, as previously stated, all the fragments from our strand appears to come from the GGG sequence broken bonds. The excitation induced by holes produced by the soft x-ray radiation tend, preferentially, to occur or migrate to these nucleobases.

5. Conclusion

The previous investigation of isolated deprotonated oligonucleotides up on absorption of energetic photons have shown qualitatively similar fragmentation pattern for each photon energy. The spectra were mainly dominated by the ionization peak due to, (TTAGGGCCGCCG-4H) $^{4-}$ at m/z =914.

The main problem we face during our experiment is the losses in the efficiency in the detection of such fragments, the negative charged fragments tend to loose electrons easily and become neutral or positive fragments which could not be observed in our experiment.

In previous studies of GCAT fragmentation, the oligonucleotide exposed to soft X-Ray suffered extensive fragmentation with nucleobases being the most abundant [9]. In their deprotonated state. In the negative mode mainly bigger fragments were observed up to a size of 10 and 9 nucleobases.

For 90 eV the main interaction is the single valence photoionization. In this process the photon removes one valence electron leaves the system excited with an excitation energy depending on the binding energy of the removed electron. Almost exclusively non-dissociative single and double ionization is observed.

In the soft X-ray range, energies close to the K-edges of N, C, and O were chosen. (See table 4). Here, the photon removes a 1s electron from the atom and that process is followed by an Auger process as explained before.

The Auger process leads to the formation of two holes in the valence band (one from the electron de-exciting into the 1s orbital, one from the emitted electron). Qualitatively, it can be assumed that twice the energy is deposited, as compared to the 90 eV case. The excitation energy is now sufficient to induce strand breaks. The photoproduct yields are dominated by multiple fragments.

Conclusions about strand sensitivity depending on the energy must be taken prudently. Neutral and positive fragments may differ by far of the negative fragments we detect, thus would completely correct or change any consideration we made during the discussion about nucleobase stability after photon absorptions.

In any case it seems that the distribution of the different atoms in the molecule play a role in the absorption cross section. Oxygen is mainly present in the backbone and sugar, Carbon is everywhere and Nitrogen is present mainly in the Guanine and Cytosine nucleobase but is not in the sugar and the backbone of the DNA.

However the main finding of the experiment is the role of the GGG sequence as hole trap. All the fragments found in the spectrums come from a breakpoint in the GGG part of the strand. Besides that, the photon energy seems not to play a role on this fact. For the whole range of energies recorded same fragments appear. So, although the distribution of the different atoms in the molecule will play a role in the absorption cross section, it does not play a role in the fragmentation pattern. The excitation, wherever is occurring tend to migrate to the GGG sequence and then induce the break.

On the other hand, the lack of positive identifications in the process of obtaining of complexes of Ag21: DNA suggest that the HPLC stages and MS is very sensitive to the performance procedure. Future detection should be performed as stated in the article and the use of the same column may play an important role.

Also, the experiment should be done in a row as fast as possible, as the stability of green1 is questioned by the results we obtained. After multiples experiment we realize that Ag:Green1 may not be stable as its fluorescence reduced a factor five after storage at 4°C for five days.

The second problem we face is the concentration of the collected sample, higher concentration are needed which lead to concentration techniques. The concentration techniques may break the bond of silver cations and DNA strand leading to the loss of the complexes. Research about this should be carry out.

6. ANNEX

5.1 Parameters of the second HPLC stage:

The second stage of the HPLC in the process of obtaining f Ag_N:DNA complexes that we finally didn´t carry out is quite similar to the first. The change in the mobile phase will lead to different retention times of the complexes we have collected in the first stage.

The Mobile phase will be formed by 400mM 1,1,1,3,3,3-Hexafluoro-2-propanol, water and methanol to reach pH 7. To this end two 800mM stocks of HFIP were prepared separately in A, water and B, MeOH from 99.5+% HFIP (Acros) and adjusted to pH 7 with TEA

Solvents "A" and "B" were prepared by diluting the stock solutions to 400mM in water for the "A" component and in MeOH for the "B" component

Ag_N:DNAs would be purified using linear gradients from 10% to 50% methanol over 40 minutes; Each gradient was preceded by a 10 minute equilibration at the initial methanol percentage and followed by a 10 minute wash at 95% methanol.

5.2 Zip Tip Concentration Procure

This is chemical procure to concentrate solutions, in our case the specific method is the next one:

Fraction contains 35mM TEAA, 1µM DNA and ~10% ACN

- Pipet 10µl 50% ACN, 0.1% TFA over the zip tip
- Pipet 10µl 0.1% TFA over the zip tip
- Pipet 10µl sample and move it up and down 3 times over the zip tip
- No washing step without TEAA to prevent losses
- Repeat this last step 4 times to concentrate it 10 times
- Elute with 5µl 50% ACN, 0.1% TFA and move it up and down 3 times again. Ready.
- Spot 0.5µl onto the MALDI plate

5.3 Solution Recipe for ESI-MS

The recipe used for the Strand3 experiment is the next one:

- 800 µl MeOH
- 150 µl H2O
- 50 µl NH4OH
- 40 µ DNA stock solution 1mM concentration

5.4 GCAT Fragmentation Spectra

The fragmentation spectra of GCAT was recorded for X energy, the main different in the operation procedure with the Strand 3 is that we expose protonated DNA, this is, we are working with positive charged ions, this may play an important role due the lower stability of DNA.

We can see this easy if start by showing the spectra obtained by Olmo of the GCAT fragmentation. As we may see, the exposed ions of GCAT explodes into small fragments of one nucleobase size.

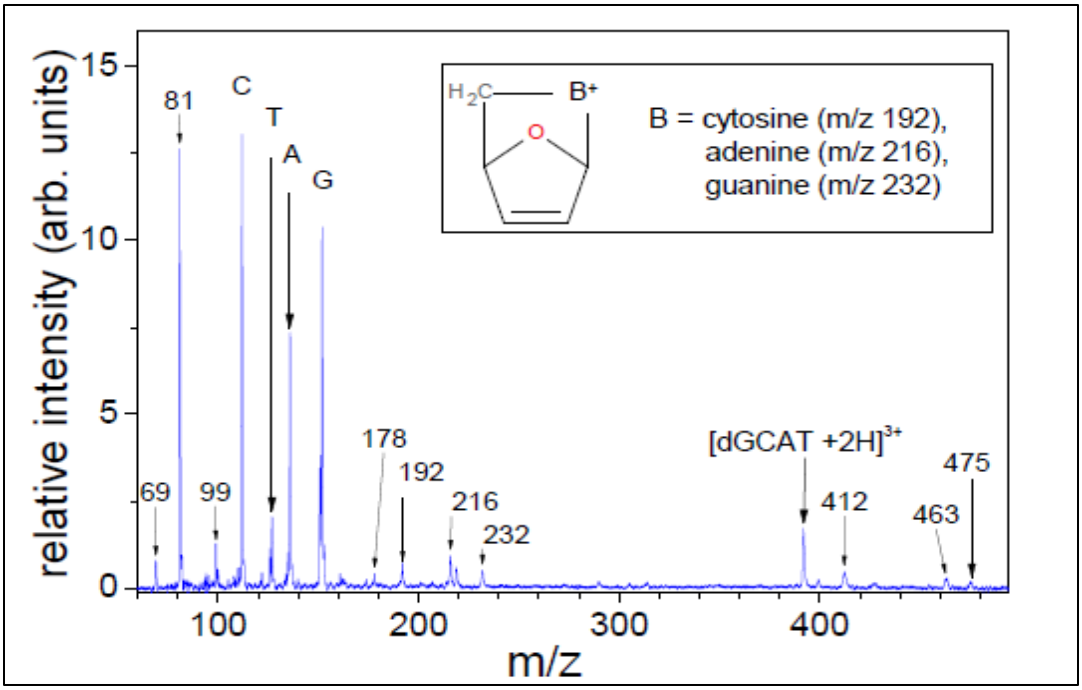

Figure 26: *GCAT positive mode fragmentation due to exposition to 40 eV photons , obtained by Olmo [9].*

The mass spectrum we obtained is pretty similar.

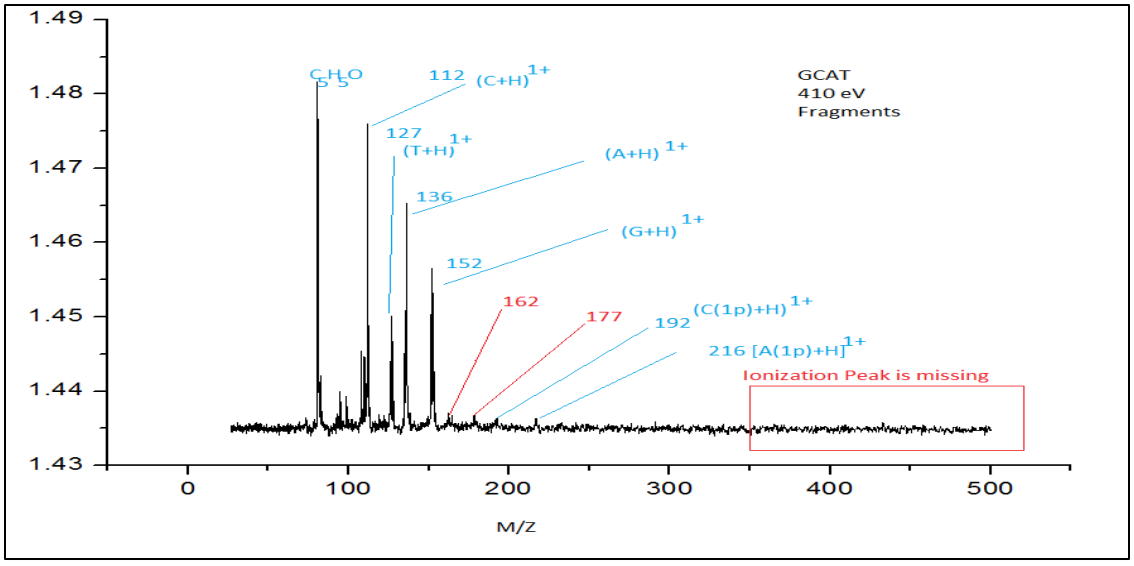

Figure 27: *GCAT positive mode fragmentation due to exposition to 410 eV photons, recorded for this thesis.*

Even if we zoom on the details of the spectrum, both spectrums are really similar. The only different we found is that to the recent spectra recorded we don't find any peaks for high masses that in fact appears in the previous spectra recorded by Olmo [9]. Also the ionization peak is missing.

A good explanation for these peaks missing is the high energy of the photons used in the second spectrum (410 eV) in comparison with the energy of the first mass spectrum (40 eV). These more energetic photons deposit more energy in the strand GCAT which tend to break the strand in small fragments, avoiding big fragments to appear.

7. Bibliography

[1] Fundamentals on HPLC, Agilent Technologies, Inc. 2009.

[2] J F Hainfeld Gold nanoparticles: a new X-ray contrast agent 2005

[3] Annals of the ICRP 2015. International Commission of Radiological Protection.

[4] ACS NANO 2013, Vol. 7, No.11

[5] NATURE 2014, 508, 133-138.

[6] SCIENTIFIC REPORTS 2011, DOI: 10.1038, srep00018.

[7] Practical Manual Guide 2016 version, QISD group.

[8] Yamashita, M. and Fenn, J. B., J. Phys. Chem., 88, 4451 (1984).

[9] Gonzalez, O. Ionization-induced fragmentation dynamics of isolated complex biomolecules (2013)

[10] Mass Spectrometry Reviews, 2010, 29, 294– 312

[11] J. Mass Spectrom. 2001; 36: 849–865.

[12] Richard B. Cole. Electrospray and MALDI Mass Spectrometry (2012)

[13] Nanomaterials 2015, 5, 180-207

[14] Adv. Mater. 2013, 25, 2797–2803

[15] Chem. Comm, 2012, 48, 5748-5750

[16] Harrison LB, Chadha M, Hill RJ, Hu K, Shasha D (2002). Oncologist 7 (6): 492–508

[17] Dole M, Mack LL, Hines RL, Mobley RC, Ferguson LD, Alice MB (1968). Journal of Chemical Physics 49 (5): 2240–2249.

[18] E. B. Guidez , C. M. Aikens , Nanoscale 2012 , 4 , 4190 .

[19] A Brief Overview of the Mechanisms Involved in Electrospray Mass Spectrometry. Paul Kebarle and Udo H. Verkerk

[20] Advanced Lab, Jan. 2008

[21] The Quadrupole Mass Filter: Basic Operating Concepts. Philip E. Miller' and M. Bonner Denton University of Arizona, Tucson, AZ 85721.

[22] Advances in Atomic, Molecular, and Optical Physics. Volume 43.

[23] Journal of Biomolecular Structure & Dynamics. Vol . 29. 3. (2011) Emilie Cauet.

[24] Nucleic Acids Research. 2007. Vol. 35. No. 15. 516-5172.